

EBERHARD KARLS
UNIVERSITÄT
TÜBINGEN



MATHEMATISCH-
NATURWISSENSCHAFTLICHE
FAKULTÄT

Advanced Practical Course

***Microchannel Plate
Detectors***

Jürgen Barnstedt

Kepler Center for Astro and Particle Physics
Institute for Astronomy and Astrophysics
Section Astronomy
Sand 1
72076 Tübingen

Published: July 5, 2019

<http://www.uni-tuebingen.de/de/4203>

Contents

1	Introduction.....	4
1.1	Background.....	4
1.2	Results of the Echelle spectrometer of the ORFEUS II mission.....	5
2	Functional principle of MCP detectors	8
2.1	Introduction.....	8
2.2	Microchannel plates and electron multiplier channels.....	8
2.2.1	Manufacturing of MCPs	9
2.2.2	Electron multiplier channels	10
2.2.3	MCP configurations.....	10
2.2.4	Gain and pulse height distribution	11
2.2.5	Sensitivity	12
2.2.6	Dark current.....	13
2.2.7	The MCPs of the <i>ORFEUS</i> detector	13
2.3	The anode.....	14
2.3.1	Introduction.....	14
2.3.2	The principle of the wedge-and-strip-anode	14
2.3.3	Alternate anode designs	16
2.3.4	The <i>ORFEUS</i> anode	17
2.3.5	Other types of anodes	18
2.4	Readout electronics.....	19
2.4.1	Theory of operational amplifiers	20
2.4.2	Charge amplifiers.....	20
2.4.3	Digital Position Analyzer.....	23
2.4.4	Data acquisition with the computer	24
2.5	Characteristics of the detector electronics.....	25
2.5.1	Noise.....	25
2.5.2	Partition Noise	25
2.5.3	Cross talk	26
2.5.4	Amplification differences	27
2.5.5	Offset	29
2.5.6	Dead time.....	29
3	Experimental setup.....	33
3.1	Detector with high voltage supply and vacuum pump.....	33
3.2	Optical bench	34
3.3	Digital Position Analyzer.....	35
3.4	Storage screen	36
3.5	Oscillograph.....	36
3.6	Computer and software	37
3.6.1	Program <i>HV-Kontrolle</i>	37
3.6.1.1	Main window	38
3.6.1.2	Test pulses.....	38
3.6.1.3	Test pulse display.....	38
3.6.1.4	Test pulse check.....	39
3.6.1.5	Gain display	39
3.6.2	Data acquisition with program <i>Acquisition</i>	39
3.6.2.1	Menu item <i>Image integration</i>	40
3.6.2.2	Menu item <i>Impulshöhe integrieren</i>	40
3.6.2.3	Menu item <i>Complete integration</i>	41
3.6.2.4	Menu item <i>Gain map integration</i>	41

3.6.3	Program <i>Druck Center One</i>	41
4	Experimentation	42
4.1	Introductory notes	42
4.2	Switch-on	42
4.3	Test pulses	42
4.4	Switch-on of the high voltage	43
4.5	Dark current	44
4.6	What does solar blind mean?	44
4.7	Pulse height distribution	45
4.7.1	Full image	45
4.7.2	Partial image	45
4.8	Outgassing	45
4.9	Flat field and gain map	46
4.9.1	Homogeneity	46
4.10	Determination of the focal length by the Bessel method	47
4.11	Dead time and efficiency	48
4.12	Linearity calibration	49
4.12.1	Setup	49
4.12.2	Measurement	49
4.12.3	Analysis	50
4.12.4	Carrying out the correction	52
4.13	Hints for writing a protocol	53
5	Literature and sources	55
6	Appendix: Natural constants	57

1 Introduction

1.1 Background

Microchannel Plate (MCP) Detectors were built since the early 1980s in the former Astronomical Institute Tübingen (AIT), which is now the section Astronomy of the Institute for Astronomy and Astrophysics. These detectors are photon counting and imaging detectors for vacuum ultraviolet light. Later these detectors were built into encapsulated glass tubes together with a photocathode for visible light. For this optical detector system a fast readout electronics was developed (Digital Position Analyser, DPA), which was connected to a PDP11 computer for data acquisition. This camera system was used for observations at large telescopes, amongst others in Asiago (Italy), on Calar Alto (Spain) and at the European Southern Observatory (ESO) in Chile.

In the middle of the 1980s the space telescope *ORFEUS* (Orbiting and retrievable Far- and Extreme-Ultraviolet-Spectrometer) was established as project and finally realised. The AIT had the scientific project management and also contributed with own hardware to this project: The MCP detectors for the Echelle spectrometer were developed and built at the AIT, as well as the corresponding electronics and the onboard computer for instrument control and data acquisition. *ORFEUS* was mounted on the reusable German satellite *ASTRO-SPAS* (*Shuttle Pallet Satellite*), which was built by the former company MBB (now part of Astrium). *ORFEUS* was flown on two space shuttle missions 1993 (4 days observation) and 1996 (14 days observation). Unfortunately during the first mission no data could be

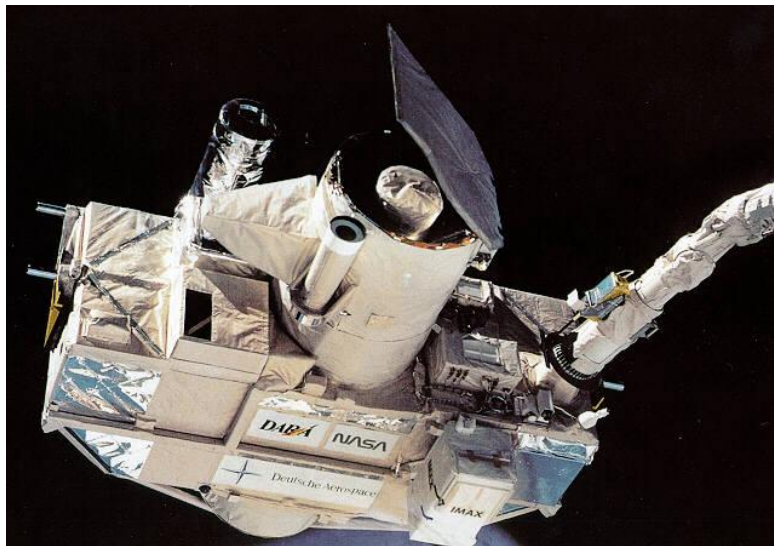


Fig. 1.1
ORFEUS during the first mission 1993 (Photo: NASA)

gathered with the Echelle spectrometer because of a malfunctioning movable mirror in the telescope, but in total this mission was very successful, as the second spectrometer, built by the University of California in Berkeley, took many measurements. The second *ORFEUS* mission was a great success and gathered during its 14 days lasting free flight a large amount of far ultraviolet spectra in the wavelength range 90 - 140 nm with a spectral resolution of 10.000 (with 17.7 days in space this also was the longest shuttle flight ever).

More details about this project may be found under:

<http://www.uni-tuebingen.de/en/4221>.

Relatively fast after the two flights it was clear that *ORFEUS* would not fly into space again. In the meantime the *ASTRO-SPAS* satellite is exhibited in the *Deutsches Museum* in München. The telescope

and the Echelle spectrometer will be exhibited in our institute, the section Astronomy at Sand 1. The detectors are working and are used for this practical course. We also are preparing now a participation with such detectors in future space projects.

In this experiment we will study the characteristics and applications of these microchannel plate detectors.

Hints for the preparation

To simplify your preparation to this experiment we interspersed some exercises in the text of the theoretical introduction. You should have answered these questions **beforehand**, as these questions will be part of the oral examination before carrying out the experiment. The solutions will be part of the protocol.

This manual was kept quite detailed in order to give sufficient background information for this experiment. The following chapters are not essential for the understanding of the experiment and may be skipped in case of short preparation time: 1.2, 2.2.1, 2.3.3, 2.3.5, 3.4, 3.5, 3.6. **But it is strongly recommended that you read chapter 4.13, p. 53 before carrying out the experiment!**

It is also very helpful, if you make yourself familiar with the functions of Excel, as part of the data analysis of this experiment will be done with Excel.

1.2 Results of the Echelle spectrometer of the ORFEUS II mission

This section will show some of the most important results achieved with the Echelle spectrometer during the second *ORFEUS* mission.

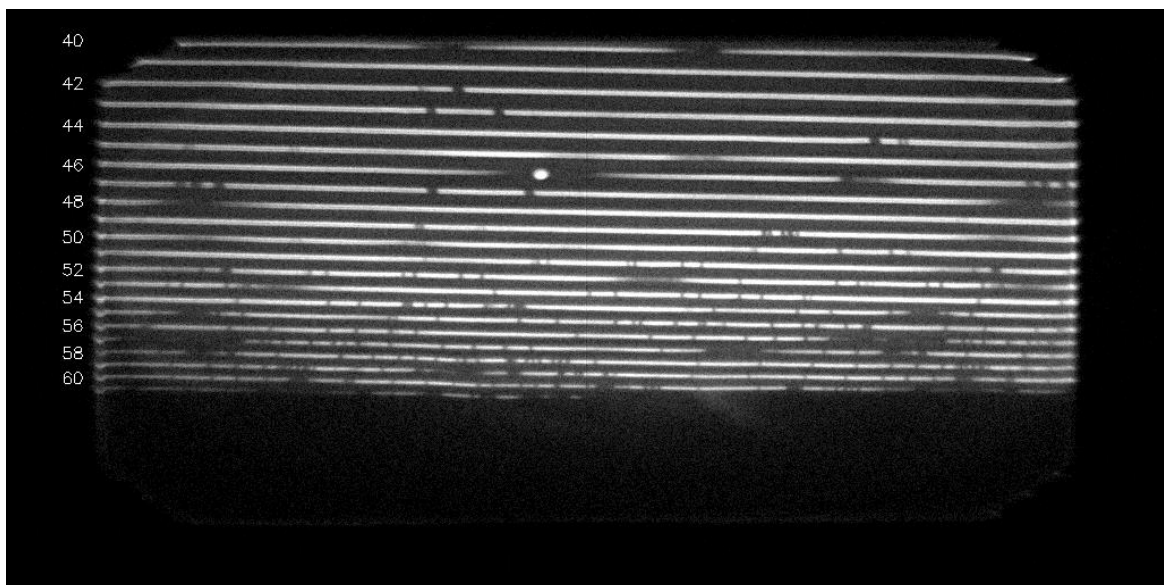


Fig. 1.2
Echelle spectrum of the white dwarf HD 93521. Left hand the orders of the Echelle grating are shown, starting with order 40 at a wavelength of about 140 nm (top left).

Fig. 1.2 shows an original measurement of the Echelle spectrometer, a spectrum of the white dwarf HD 93521. This image is not quadratic, as the data were recorded in X-direction (main dispersion of the spectrometer) with 1024 pixels, while in Y-direction (cross dispersion) only 512 pixels were recorded, which was sufficient to separate the individual spectral orders (numbered from 40 to 60 in this image). The wavelength range starts at about 90 nm (order 61, centre) and ends at about 140 nm (order 40, top left).

An Echelle spectrometer comprises two different gratings. The high spectral resolution is produced by a Echelle grating, which operates in high spectral orders (here: orders 40 – 61). As these diffraction orders overlap each other, a second grating (cross disperser) is used to achieve dispersion with a low spectral resolution perpendicular to that of the Echelle grating. Thus the overlapping orders of the Echelle grating are arranged below each other on the detector, and the individual orders run slightly tilted across the image.

The image shows already quite clearly some absorption lines as dark areas. You may also distinguish two different kinds of absorption lines: broad and narrow ones. The broad lines are broadened due to the Doppler Effect. They originate from hot gases and are therefore of stellar origin (stellar atmosphere). The narrow lines conversely originate from cold gas clouds, which are located somewhere in interstellar space between earth and the observed star. A closer look reveals that some of the narrow lines are double lines. These are Doppler shifted lines which means, that the light passed through two different gas clouds which move with different velocities relative to the earth. Fig. 1.3 shows a plot of a section of this spectrum with absolutely calibrated flux and wavelength scales together with many identified absorption lines. A total of more than 300 different absorption lines were identified (Barnstedt et al. 2000). Very remarkable is the multitude of nearly 200 absorption lines of molecular hydrogen H_2 in this spectrum, which originate from at least two different interstellar gas clouds. H_2 is observable only in this *ORFEUS* wavelength range. Even some stellar atmospheres contain molecular hydrogen H_2 and its ions H_2^+ . These short living molecules form at high gas pressure and are called quasi molecules. With *ORFEUS* they could be measured for the first time in a wavelength range below 120 nm.

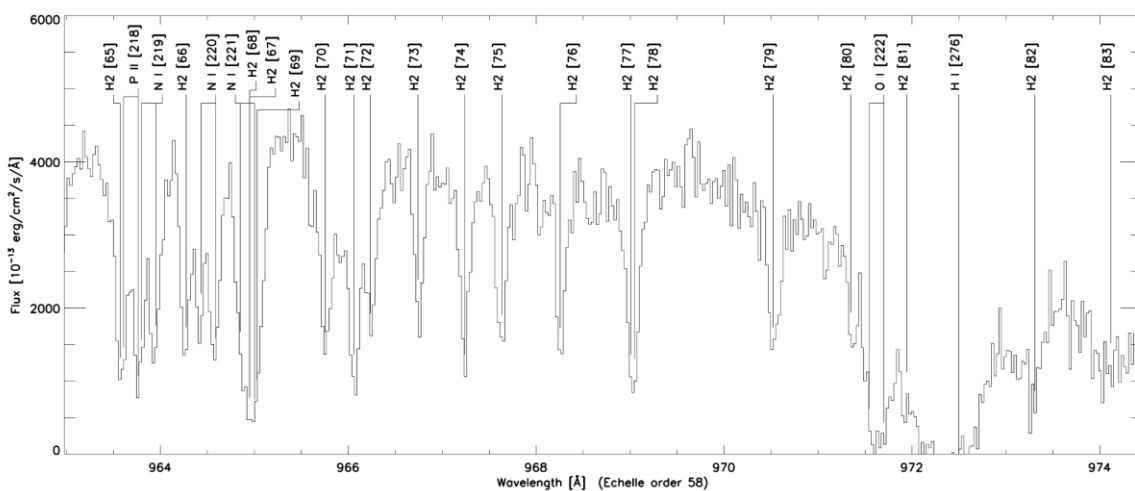


Fig. 1.3
Section of the Echelle spectrum of the white dwarf HD 93521. The identified absorption lines are marked: H_2 = molecular hydrogen H_2 , $O I$ = neutral oxygen, $N I$ = neutral nitrogen, $P II$ = single ionised phosphorus, $H I$ = neutral hydrogen (line of the Lyman series, Lyman- γ = 972.537 nm, stellar line). (Source: Barnstedt et al. 2000)

Also in the spectra of stars of the two Magellanic Clouds cold H_2 could be detected. The absorbing gas clouds are high velocity clouds in the halo of our own galaxy and therefore they have nothing to do with the Magellanic Clouds. In one case even absorption lines of highly excited states were observed, which indicated an illumination of this gas cloud with UV light. Such high excitations were observed with *ORFEUS* for the first time.

Besides hydrogen in some of the spectra also deuterium could be found. Deuterium was produced during the Big Bang and was dissipated later by stellar burning processes. Thus the amount of deuterium decreases during the development of the universe. With *ORFEUS* the abundance of interstellar deuterium in the direction of two stars could be determined – for the first time from the measurement of 5 or 6 absorption lines. This allowed for the estimation of the interstellar D/H ratio. The values were within the range of previously known measurements.

From spectra of the Large Magellanic Cloud a lower limit for the H_2/CO ratio could be estimated. CO is quite common in space and can also be observed at radio frequencies, in contrast to H_2 . Therefore CO can be observed rather easily all over the space and it is assumed that H_2 occurs there, where also CO occurs. So a direct estimation of the H_2/CO ratio is important to deduce the amount of H_2 from CO measurements.

By observation of emission lines of fivefold ionised oxygen (O VI, visible only in the *ORFEUS* wavelength range) of symbiotic stars it could directly be shown, that this radiation produces emission lines in the visible spectral range by Raman scattering. The oxygen emission lines are absorbed as hydrogen Lyman- α line and the excess energy is emitted as line in the visible range. This process was already known, but it was the first time, that it could directly be observed.

In general by observation of O VI very hot gases of about 200 000 K can be detected. With *ORFEUS* this detection succeeded also for gas clouds in the halo of our galaxy.

Finally for the first time it was possible to observe HD molecules in the Small Magellanic Cloud.

A more detailed summary can be found on this web page (in German):

<http://www.uni-tuebingen.de/en/4319>

2 Functional principle of MCP detectors

2.1 Introduction

The detectors we are dealing with in this experiment are photon counting, imaging detectors. They register single photons, estimate the position of each photon and store the photons coordinates in a computer.

The important parts of such a detector are one or more microchannel plates (MCPs) and a wedge-and-strip anode (WSA).

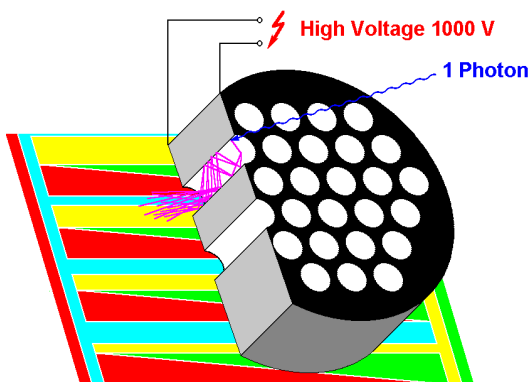


Fig. 2.1
Functional principle of an MCP detector

MCPs are plates which comprise microscopic small bundled electron multiplier channels. They are made of glass. The upper and lower surfaces of these plates are metallised electrodes to which a voltage of typically 1000 V is applied. The inner surfaces of the microchannels are semiconducting. A weak current through the channel surface produces a homogeneous electrical field inside the channel. A UV photon hitting the channel surface will release a photo electron (under vacuum). The strong electrical field will accelerate the electron towards the back end of the channel. This electron will hit the channel wall and may release two

(or more) electrons. Thus an electron avalanche will occur in the channel and finally leave the channel. About 10^4 electrons may leave one channel as electron cloud.

This electron cloud will hit the wedge-and-strip anode. The anode comprises a gold layer on a quartz substrate, into which a pattern of 4 intersecting electrodes is etched. Thus the impinging electron cloud will disperse over all 4 electrodes. From the ratios of the amount of electrons hitting all 4 electrodes the centre of gravity of the electron cloud can be determined. This gives the coordinate of the registered photon.

The charges collected by the 4 electrodes are electronically amplified by sensitive charge amplifiers and transmitted as bipolar voltage pulses to the analysing electronics. The peak values of the voltage pulses are digitised by analogue to digital converters. The further computation of the 4 charge values into position coordinates is done digitally. The data acquisition computer receives the values and stores them.

2.2 Microchannel plates and electron multiplier channels

The following sections cover manufacturing, function and characteristics of MCPs and electron multiplier channels.

2.2.1 Manufacturing of MCPs

Microchannel plates are made by glass fibre technology. Base material is a glass rod assembled from a hollow tube of non-etchable glass and a core of etchable glass. These rods are heated and drawn to a diameter of about 0.8 mm. Bundled to a hexagon rod and drawn again, the final hexagons are fused together to the desired diameter (see Fig. 2.2).

The resulting boule is cut into thin slices

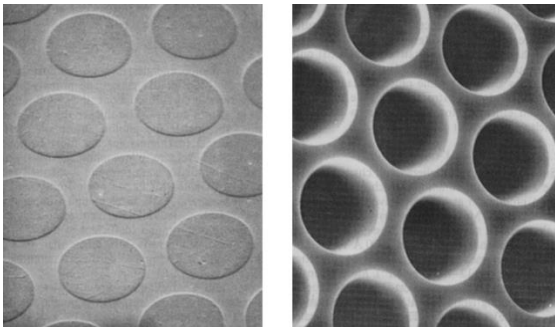


Fig. 2.4

Scanning electron microscope image of an MCP surface before (left) and after (right) etching of the channels (source: Wiza, 1979)

which will later become the MCPs. They are polished and finally the core material of the original rods is etched away so that the channels are formed. These channels typically measure $12.5\ \mu\text{m}$ in diameter with a centre-centre distance of $15\ \mu\text{m}$. Channel diameters of $8\ \mu\text{m}$ or even $4\ \mu\text{m}$ can be realised nowadays. By treatment in a hot hydrogen atmosphere the channel walls become semiconducting and the desired secondary electron emission characteristic is achieved. Under vacuum the metal electrodes are evaporated onto the two surfaces to get electrical contact to the individual channels.

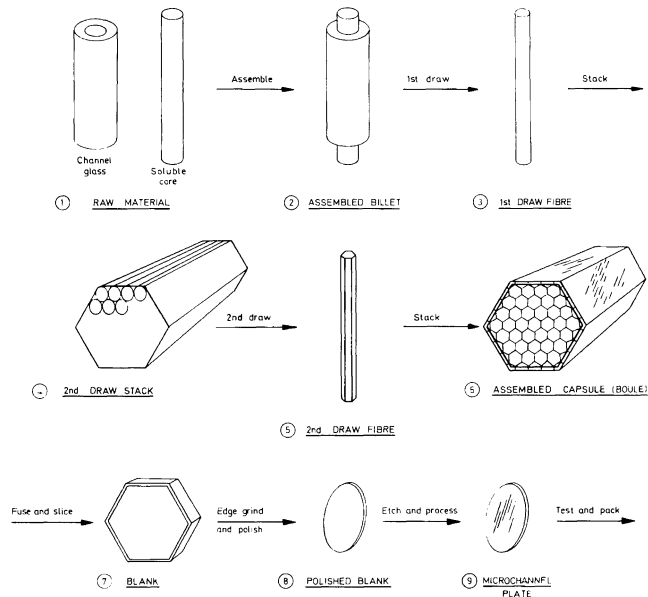


Fig. 2.2

Steps of the MCP manufacturing (source: VALVO, Technische Informationen für die Industrie, Microchannel plates, 1976)

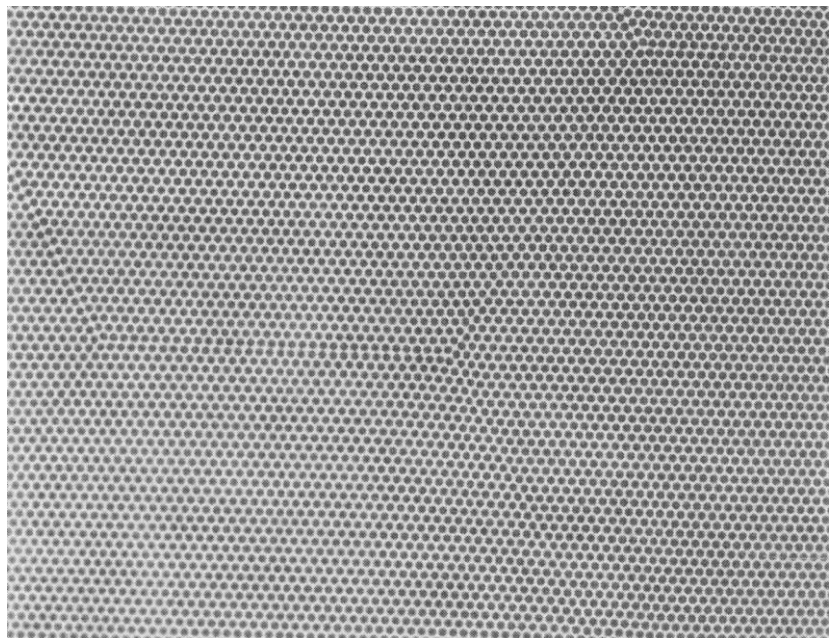


Fig. 2.3

Microscopic view of an MCP surface. The boundaries of the hexagon bundles are clearly visible. (Source: Vallerga et al., 1989)

2.2.2 Electron multiplier channels

Each channel of a MCP works as an electron multiplier channel. The impinging primary radiation releases a secondary electron at the beginning of the channel which is accelerated by the applied high voltage and will release 2 or more electrons when hitting the channel wall again (Fig. 2.5). Thus an electron avalanche is generated in the channel which leaves the channel as electron cloud and can be electronically registered as charge pulse. So called Channeltrons work accordingly (Fig. 2.6). The channel entrance of Channeltrons usually is funnel-shaped enlarged to enlarge the sensitive area. The channel itself is circular curved to avoid ion feedback. Ion feedback occurs, when the electron cloud ionises residual gas atoms at the end of the channel. These



Fig. 2.6
Different Channeltron types
(source: Galileo Electro-Optics Corporation)

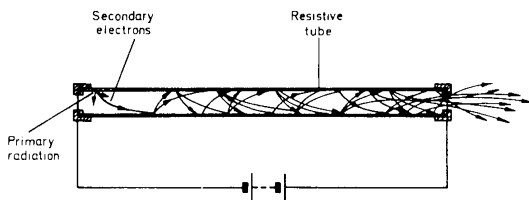


Fig. 2.5
Electron multiplier channel (source: VALVO, Technische Informationen für die Industrie, Microchannel plates, 1976)

positively charged ions might be accelerated back to the beginning of a straight channel where they could release new pulses. This would result in an instable behaviour and should therefore be avoided. Curved channels prevent ions from reaching the beginning of the channel und thus prevent ion feedback.

2.2.3 MCP configurations

MCPs are available also with curved channels which allow for a higher gain than normal MCPs without occurrence of ion feedback. But usually several stacked MCPs are used to achieve high gain. The channels of each MCP are tilted ($8^\circ - 15^\circ$) against the MCP normal and the channels of successive MCPs are tilted to opposite directions. 2 MCPs in this configuration are called chevron configuration and 3 MCPs Z-configuration (Fig 2.7). The angled arrangement of the channels effectively suppresses the ion feedback.

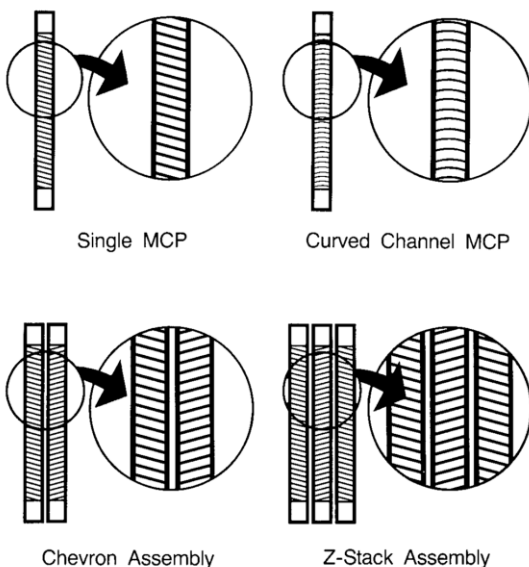


Fig 2.7
MCP configurations (source: Galileo Electro-Optics Corporation)

Configuration	Max. Voltage	Gain	Pulse height distribution
Single-MCP	1000 V	10^3-10^4	exponential
Curved Channel	2400 V	10^5-10^6	50% FWHM
Chevron conf.	2000 V	10^6-10^7	120% FWHM
Z-configuration	3000 V	10^7-10^8	80% FWHM

Table 2.1
Properties of MCP configurations (source: Galileo Electro-Optics Corporation)

Exercise 1:

Give two reasons for the fact, that MCPs can be operated only under vacuum. (What would happen, if you would try to operate a MCP under atmospheric pressure?)

2.2.4 Gain and pulse height distribution

Single MCPs are operated best in an analogue mode. In this mode the output current of a MCP is registered, which is proportional to the incoming photon flux. With this method one cannot detect single photons; it corresponds to a standard photomultiplier operated in a conventional analogue mode. Analysing single pulses in this mode one will find that the pulse height distribution shows an exponential decay (Table 2.1), i.e. weak pulses occur very frequent, whereas strong pulses are quite rare.

For a counting mode, which registers preferably all incoming photons, a configuration is needed that produces in an ideal case a fixed pulse height for each event. In practice you will get pulse height distributions which show a more or less pronounced maximum. Such pulse height distributions are achieved only with very high gain configurations. In that case the electron density is very high at the end of the channel such that a counter electrical field builds up and the electron avalanche will not increase further. This results in a saturation of the gain in this channel and thus all pulses nearly get the same amount of electrons. Such a pulse height distribution is characterised by the full width at half

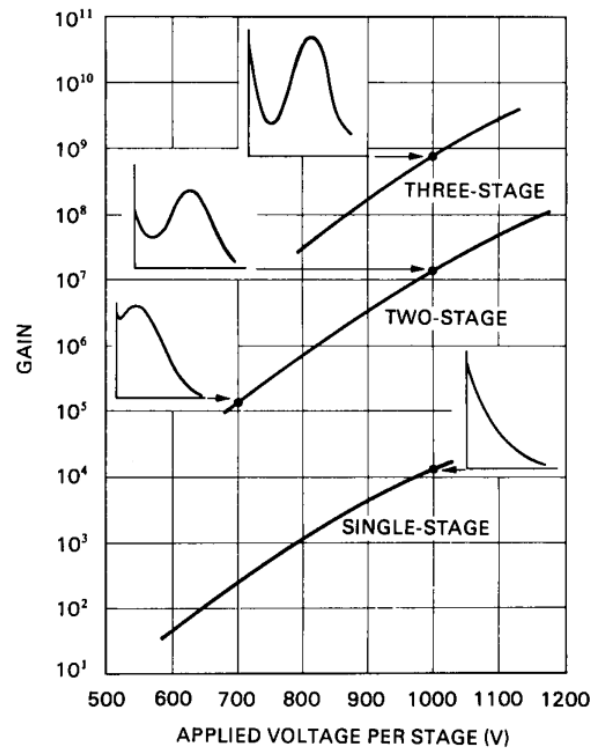


Fig. 2.8 Relation between Gain, pulse height distribution, voltage and MCP configuration (source: Hamamatsu)

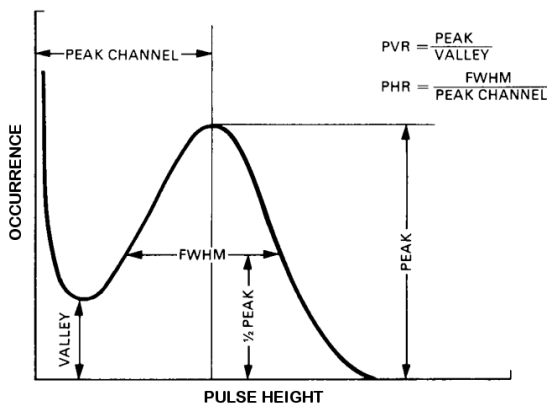


Fig. 2.9 Pulse height distribution: Definition of Full Width at Half Maximum, FWHM (source: Hamamatsu)

maximum (FWHM, see Fig. 2.9). Usually the width is related to the peak position of the distribution (modal gain) and given in percent of this position, the value of which may be larger or smaller than 100%. Alternatively the width may be related to the mean gain. It should be noted to which kind of gain the width is related if given in percent, as these two values are not identical if the distribution is not symmetrical – which is the normal case for pulse height distributions.

Small relative widths are usually desired, as the trigger threshold of the pulse detection electronics

may be set well above the noise level while still detecting practically all pulses.

2.2.5 Sensitivity

Fig. 2.10 shows details of the surface characteristics of the MCP channels. Electrons may be released from a depth up to 200 Å (20 nm). MCPs are therefore sensitive to ionising radiation with a penetration depth between 1 nm and 20 nm. This can be ultraviolet and X-ray radiation as well as electrons and ions. For UV radiation the long wavelength limit is at about 150 nm (about 8 eV), for longer wavelength photons the sensitivity rapidly decreases. The high energy limit for X-rays is at about 0.1 nm (12 400 eV), as photons with higher energy will penetrate deeper into the material than 20 nm and will therefore hardly release electrons (Fig. 2.11).

The feature that MCPs are not sensitive to visible light is called “solar blind”. This is for UV and X-ray detectors used in space a quite essential characteristic. Sun light is usually present as stray light in the optics of the instruments and also is more intense by several orders of magnitude as the radiation to be measured. Therefore stray light suppression is essential as well as using solar blind detectors to detect weak UV or X-ray radiation.

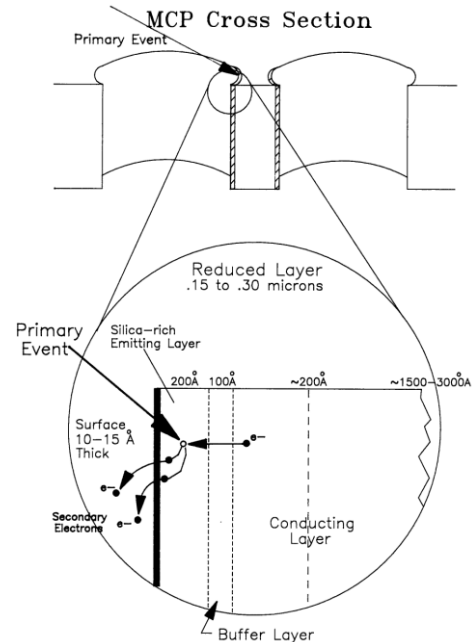


Fig. 2.10
Detail of the surface of a MCP channel
(source: Galileo Electro-Optics Corporation)

The sensitivity for UV photons may be increased by photo cathodes. Usually the photo cathode material is applied directly onto the MCP surface. Important photo cathode materials are shown in Table 2.2.

A disadvantage of these photo cathodes is their sensitivity against air. They are hygroscopic and may react with oxygen. As a rule of thumb, the materials are more sensitive to air the longer the wavelength limit of their UV sensitivity is. KBr may be exposed to air for several hours before a degradation is seen. CsI will degrade after a few minutes, while Rb₂Te and Cs₂Te may not be exposed to air at all.

A further increase in sensitivity may be achieved by applying an electrical field in front of the MCP.

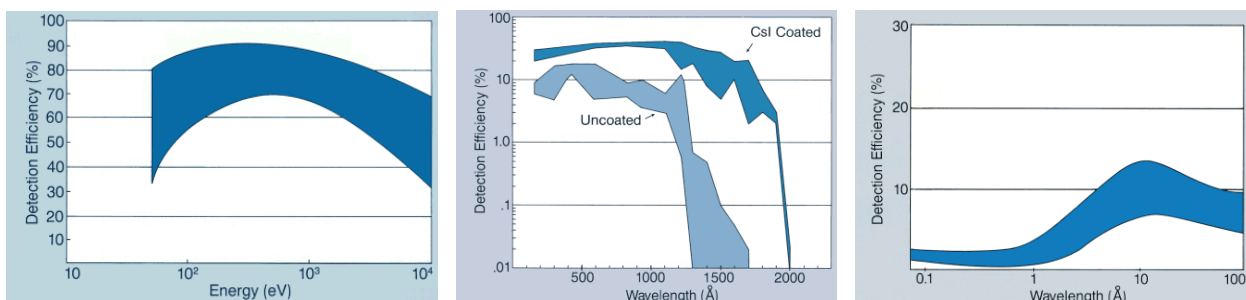


Fig. 2.11
Sensitivity of MCPs for electrons (left), UV photons (middle, with and without CsI photo cathode) and X-ray photons (right) (source: Galileo Electro-Optics Corporation)

Electrons, which are released on the MCP surface between the channels, will be forced back into the channels by this field – otherwise they would leave the MCP surface in the opposite direction and would be lost. Thus the sensitivity of the detector may be increased by 30 %. In case of the *ORFEUS* detector the electrical field is applied by a mesh mounted in front of the MCPs. This mesh causes a photon loss of about 10 %, leaving a total gain of about 20 % in sensitivity.

Material	long wavelength limit [nm]
potassium bromide (KBr)	155
caesium iodide (CsI)	200
rubidium telluride (Rb ₂ Te)	300
caesium telluride (Cs ₂ Te)	350

Table 2.2
Photo cathode materials

2.2.6 Dark current

Even an absolutely dark MCP will produce pulses. This dark count rate is typically 0.2 - 1 counts / s cm². About 90 % of this dark current is caused by radioactive decay of components of the MCP glass (β -decay of ⁴⁰K, half life $1.28 \cdot 10^9$ years, Fraser 1989). As these pulses are released not only at the beginning but arbitrarily within a channel, the pulse height distribution has no maximum but shows a roughly exponential trend.

2.2.7 The MCPs of the *ORFEUS* detector

The MCPs for the *ORFEUS* detector were custom-made by Hamamatsu Photonics. Three MCPs in a Z-configuration are used. This configuration achieves a gain of 10^7 to 10^8 electrons per photon. The first two MCPs have a thickness of 1.0 mm, while the third MCP has a thickness of 0.6 mm. The diameter of the MCPs is 60 mm. The channels have a diameter of 12 μ m and a centre to centre distance of 15 μ m (see also Exercise 2). With a MCP thickness of 1 mm (= length of channels) the ratio of length to diameter of the channels is about 80:1. The first MCP carries a KBr photo cathode. The size of the sensitive area of the detector is limited by a specially designed MCP electrode to 40 x 40 mm² (Fig. 2.12).

A special feature of the *ORFEUS* detector is, that the MCPs are insulated against each other with a distance of 0.3 mm. This allows for an individual high voltage supply of the single MCPs and also to apply an acceleration voltage between the MCPs. By variation of the high voltage of the third MCP the gain of the detector is adjusted.

1 cm in front of the MCPs a mesh is mounted to which a voltage of 500 V with respect to the first MCP is applied. This produces an electric field of 50 V/mm in front of the

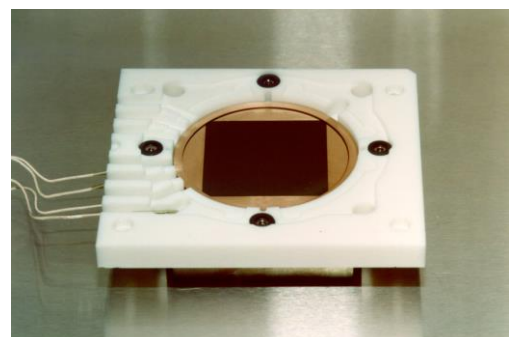


Fig. 2.12
ORFEUS detector: View onto the backward electrode of the first MCP which restricts the sensitive area of the detector to 40 x 40 mm². Additionally the insulated electrode of the second MCP can be seen.

photo cathode. This electric field causes photo electrons, which are released on the MCP surface between the channels, to be deflected into the channels.

Exercise 2:

Calculate the fraction of the channel openings with respect to the total MCP area (open area ratio, OAR) in percent.

2.3 The anode

2.3.1 Introduction

The anode is mounted behind the MCPs. It has electrodes that collect the electrons leaving the MCPs. The function of the anode is to code the incoming charges in such a way, that it is possible to estimate the position of the original photon that released the charge pulse.

The originally by H.O. Anger (Martin et al., 1981) developed wedge-and-strip-anode (WSA) is based on the principle of charge division, which allows for the calculation of the position coordinates from the ratios of the collected charges.

The distance between MCP and anode is about 7 mm. Between MCP and WSA there is a very homogeneous electric field, which accelerates the electrons onto the WSA. Due to the relative large distance between MCP and WSA the electron cloud expands such that the diameter of this cloud is a few millimetres.

2.3.2 The principle of the wedge-and-strip-anode

A wedge-and-strip-anode comprises a quartz plate with a thin gold layer into which a periodic structure of four different interlaced electrodes is etched. Two of these electrodes form a pair of complementary wedges, while the other two form a pair of strips, the summed height of which is constant, but the ratio of their heights varies over the anode. Fig. 2.13 clarifies how the X-position is coded by the wedges and how the strips code the Y-position.

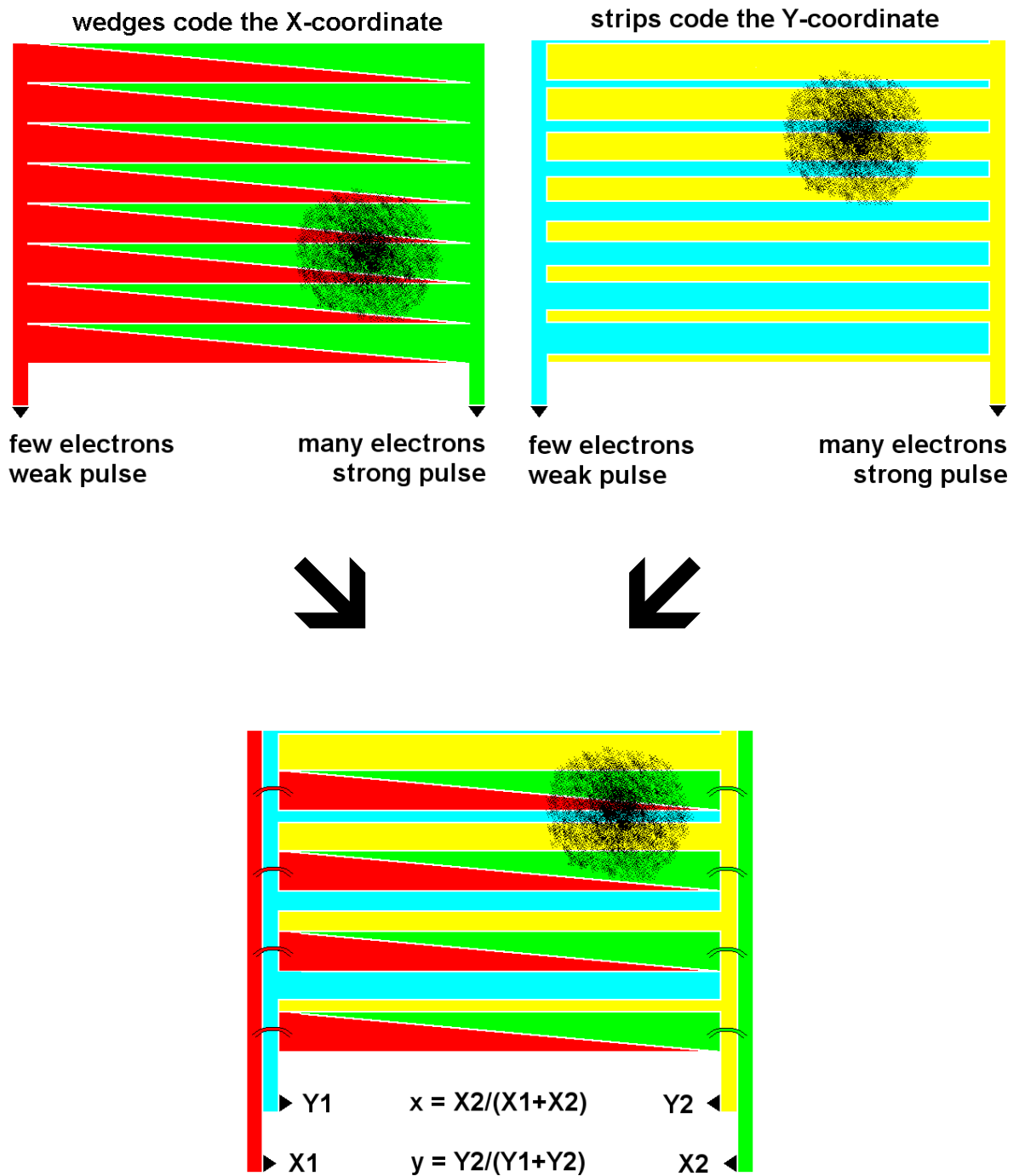


Fig. 2.13
Functional principle of a wedge-and-strip-anode. The coordinates (x,y) of the centroid of the charge cloud are calculated from the ratios of the charges X1, X2, Y1 and Y2.

A precondition for a linear encoding of the position by the anode is that the width of the electron cloud is about twice the period width of the anode structure. By choosing the correct distance and the correct field strength between anode and MCP the width of the electron cloud can be adjusted accordingly. If the width of the electron cloud is too small, periodic distortions will appear in the recorded image, which reflect the periodic structure of the anode. If the width of the electron cloud is too large, distortions in the border area of the image will be larger.

The distortions in the border area can not completely be avoided; they are caused by the necessary width of the electron cloud. The design of the anode of the *ORFEUS* detector largely avoids these border distortions, as the active anode area is about 10% larger than the active imaging area of the detector. The border distortions may be further minimised by extending the anode structure beyond the active area with constant parameters (Fig. 2.14).

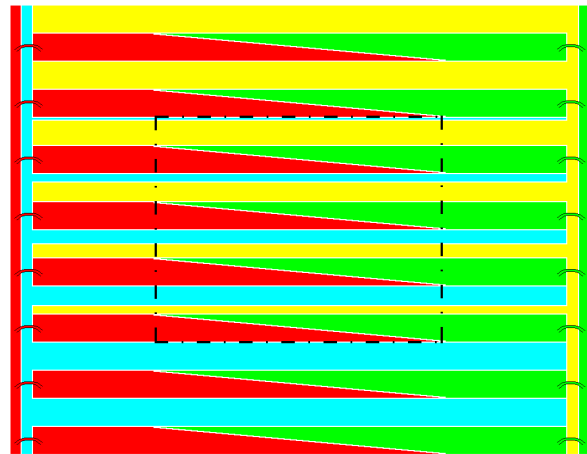


Fig. 2.14
Principle of a wedge-and-strip anode with optimised design. The active anode area is indicated by the dash-dotted line.

Exercise 3:

For achieving a good imaging quality it is important to keep the capacitance between the 4 electrodes as small as possible. Why should the substrate of the anode therefore preferably made from quartz instead of ordinary glass? (Quartz of trademark Suprasil was used.)

2.3.3 Alternate anode designs

A disadvantage of the 4-electrode anode design is that electrical contacts are needed on the anode surface for bridging the conductor paths of the strips on each side of the anode (see Fig. 2.13). For the *ORFEUS* anode this problem was solved by the use of bonding wires, a technique known from microelectronic

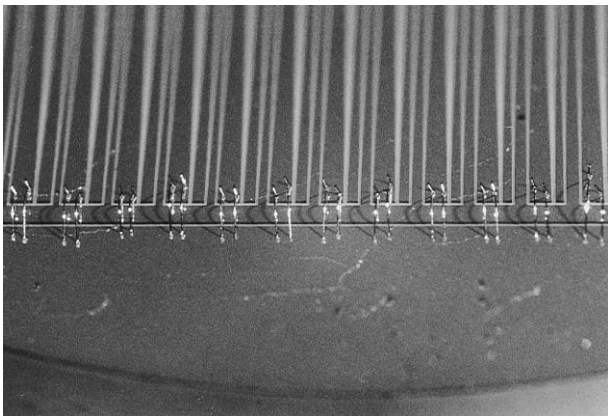


Fig. 2.15
Wedge-and-strip anode of an optical MCP detector. The bonding wires are visible, which connect the wedges with their conductor path.
(Source: Barnstedt 1985)

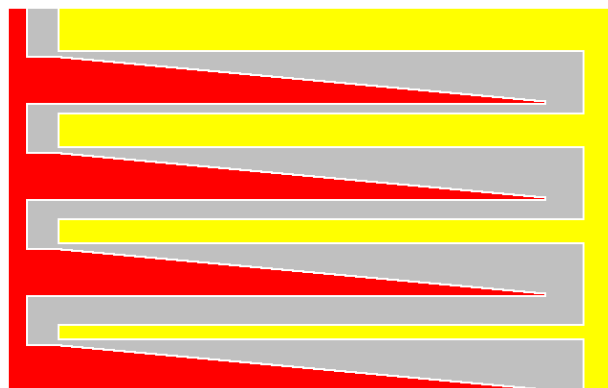


Fig. 2.16
Principle of a 3-electrode wedge-and-strip anode. Calculation of the coordinates:

$$x = 2Q_{\text{wedge}} / (\Sigma Q)$$

$$y = 2Q_{\text{strip}} / (\Sigma Q)$$

fabrication (Fig. 2.15). This could be avoided by using a 3-electrode anode design, in which one wedge electrode and one strip electrode are combined to one common Z-electrode which runs in a meandering course across the anode (Fig. 2.16). For calculating the position coordinates it has to be considered that in the original design of the 4-electrode anode the area of both wedges is the same as the area of both strips. Thus both the two wedges and the two strips get half of the total charge ΣQ . A disadvantage of this 3-electrode design is that the above described method of optimising the

anode design by extending the anode structure beyond the active area cannot easily be applied, as the width of the Z-electrode becomes nearly zero in the upper left corner. Therefore the resistance of the conductor path cannot be neglected, which results in further image distortions.

2.3.4 The *ORFEUS* anode

Table 2.3 shows the technical data of the anode of the *ORFEUS* detector. This anode was manufactured by the company Heidenhain GmbH according to our specifications. Fig. 2.17 shows the *ORFEUS* anode in its mounting. The four electrical connections were glued with an electrically conductive adhesive onto the gold coating.

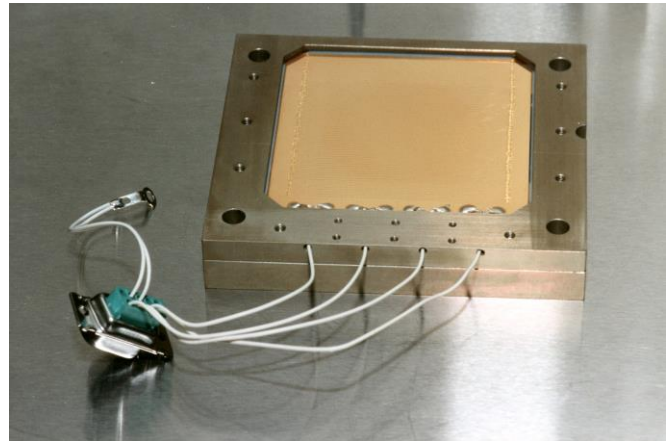


Fig. 2.17
Wedge-and-strip-anode of the *ORFEUS* detector.

Substrate	Quartz (Suprasil)
Size (length x width x thickness)	70 mm x 70 mm x 5 mm
Active area	44 mm x 44 mm
Width of passive area	7 mm
Period width (2 wedges + 2 strips)	1 mm
Distance between electrodes	20 μm
Conducting material	Gold, 2 μm

Table 2.3
Technical data of the anode of the *ORFEUS* detector

The *ORFEUS* anode comprises two additional electrodes on the back side of the quartz substrate with an area of 3.2 cm² each. They are located at two opposite corners of the active anode area. They form a capacitance with the anode so that rectangular test pulses could be coupled onto the anode by these electrodes. The falling edge of such pulses simulates an impinging electron cloud while the rising edge produces inverted pulses which are suppressed from being evaluated by the electronics. The test pulse

Exercise 4:

Calculate the capacitance of a test pulse electrode with respect to the anode (thickness of the anode: see Table 2.3). What voltage must a test pulse have to simulate a charge cloud with 10^7 electrons?

electronics can selectively produce pulses on one of the two electrodes (bottom left LU = *links unten*, or right top RO = *rechts oben*) with 3 different pulse heights.

2.3.5 Other types of anodes

For the sake of completeness further position sensitive anodes for MCPs shall be presented here (without claiming real completeness).

Resistive anode

The resistive anode comprises a homogeneous resistive layer on a supporting substrate. It covers a quadratic area, but the borders are made from circular shaped linear resistors which have a defined resistance per length unit. The charges are collected from the four corners (Fig. 2.20). Similar to the wedge-and-strip anode the position is calculated from the ratios of the charges. Disadvantages of the resistive anode are:

- Sensitivity against inhomogeneity of the area resistance
- Resistive noise is amplified by the charge amplifiers and degrade the signal to noise ratio
- The active area of the anode cannot used completely for imaging

MAMA detectors

MAMA detectors (Multi Anode Microchannel Arrays) comprise a MCP with curved channels and as anode a 2-dimensional array of 1024 electrode strips. The 1024 electrodes (in both X- and Y-direction) are interconnected into 66 groups, so that a 1024 x 1024 Pixel anode needs 132 charge amplifiers. A coincidence logic determines from the amplifiers that are hit at the same time the real position of the event. The rather complex manufacturing of the anode and electronics make this type of detector interesting for space missions only. For the time being this detector type is used in the *Space Telescope Imaging Spectrograph* (STIS) on board the *Hubble Space Telescope* (HST) (Danks et al. 1992).

Fig. 2.19 shows the construction of a MAMA detector. Key: ① MCP with curved channels, ② Coincidence anode array, ③ Quartz substrate, ④ upper electrode layer, ⑤ lower

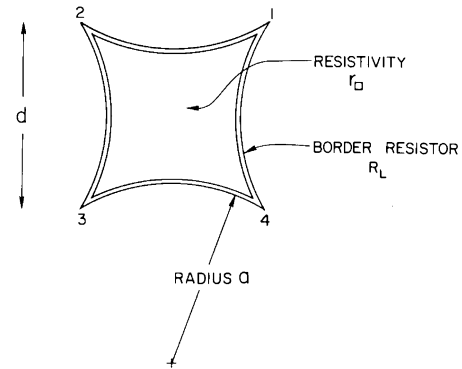


Fig. 2.20
The geometry of a resistive anode (source: Lampton et al., 1979)

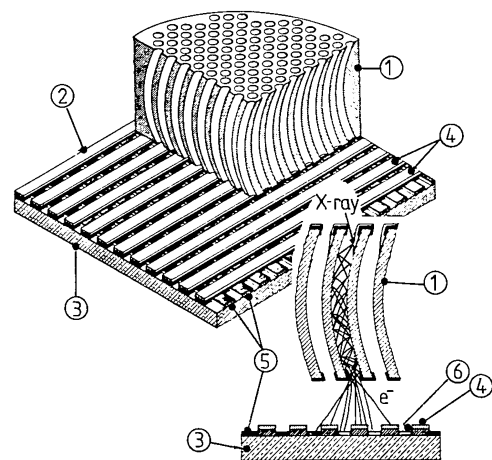


Fig. 2.19
Construction of a MAMA detector (source: Fraser, 1989 – courtesy J.G. Timothy)

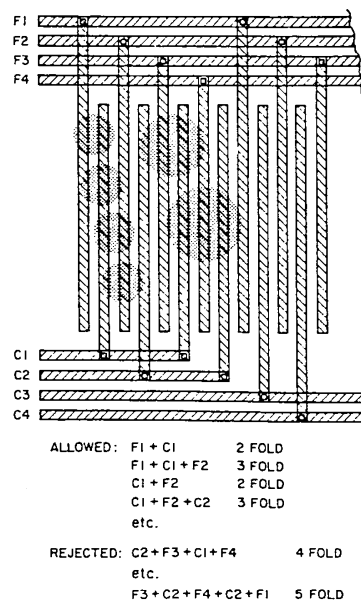


Fig. 2.18
Principle of the position coding of the MAMA detector (source: Fraser, 1989 – courtesy J.G. Timothy)

electrode layer, © insulating layer of SiO₂.

Delay Line Anodes

Delay line anodes make use of the principle of an electronic R-C circuitry which is able to slow down the propagation of pulses. The propagation time of electronic signals is reduced so that it can be measured even at small distances. Thus the distance covered by a signal may be estimated from the travelling time of that signal. If a signal is injected at a certain position of a delay line, the difference in arrival times at both ends of this line can be used to estimate the exact position of the injection of this signal. The precision in the position determination depends only on the characteristic propagation time of the signal and on the precision of the time measurement, but not on the length of the line.

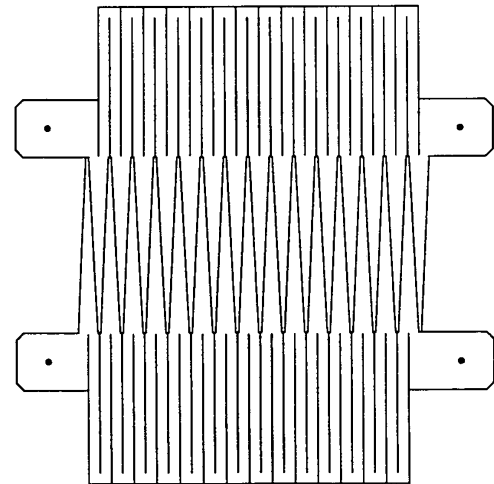


Fig. 2.21
Principle of a Double Delay Line Anode
(source: Siegmund, 1992)

A double delay line anode was developed by the *Space Sciences Laboratory* of the University of California at Berkeley. The anode allows for a 2-dimensional position encoding, at which one axis is coded by the delay line principle and the other axis is coded by a wedge anode. The advantage of this design is a planar geometry of the anode structure, which avoids crossing tracks like the *MAMA* detector. Another advantage is the high spatial resolution in direction of the delay line.

Fig. 2.21 shows the layout of this anode. The Y axis is coded by wedges, but the ends of those wedges are connected by R-C elements. These R-C elements are implemented as meandering conductors and are directly etched into the anode surface. Thus there are two delay lines, one for the upper and one for the lower wedges. A critical point is that both delay lines have to have exactly the same characteristic propagation time.

Such detectors can be favourably used for applications which need a high spatial resolution in just one axis while for the other axis a lower resolution is sufficient. A typical application is a detector for spectrographs which need high resolution in dispersion direction (high spectral resolution), while perpendicular to this direction a low resolution is needed only to distinguish between different spectral orders or for a simple spatial resolution if a long entrance slit of the spectrometer is used.

Such detectors were used amongst others in the second instrument of the *ORFEUS* telescope, the Berkeley Extreme and Far-Ultraviolet Spectrometer (*BEFS*) (Hurwitz et al., 1988), and in the *FUSE* satellite.

2.4 Readout electronics

The readout electronics registers the charge pulses from the anode and calculates from the ratios of these charges the position of the centre of gravity of the charge cloud which is registered as position of the incoming event. This electronics comprises charge amplifiers which convert charges into voltage pulses.

These voltage pulses are fed into the Digital Position Analyser (DPA), which digitises these pulses and digitally carries out the calculation of the position. The data are finally transferred to a computer.

2.4.1 Theory of operational amplifiers

The three-cornered symbols in Fig. 2.22 represent operational amplifiers (short: op-amp). These op-amps are electronic standard components. They are available in countless designs with optimized characteristics for very different applications. The theory of these op-amps however is very simple:

They have two inputs and one output. The inputs are marked with a plus and a minus symbol („+“: non-inverting input, „-“: inverting input). The right angle of the triangle is the output. The theoretical function of an op-amp is the following: It amplifies the voltage difference between the two inputs by infinity (practically the amplification factors are very large). This fact leads to a simple conclusion: A meaningful output signal can be achieved only, if the voltage difference between the two inputs is zero, i.e. if both input signals are at the same potential. Therefore op-amps are wired such that there is a feedback from the output to the inverting input, so that a change

in the input voltage will be compensated subsequently. In a frequently used circuitry the non-inverting input (+) is connected directly to ground (zero potential). Thus the inverting input (-) will actively also be put to zero potential (virtual ground). The charge amplifiers described in the following operate according to this principle and are wired as integrators (Tietze/Schenk, chap. 12.4).

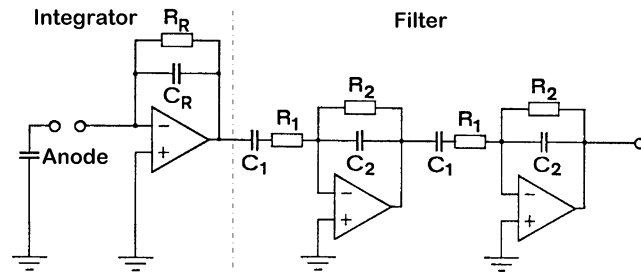


Fig. 2.22
Principle of the charge amplifiers: Integrator circuitry with electronic filter

2.4.2 Charge amplifiers

Fig. 2.22 shows the principle circuitry of the charge amplifiers. The anode is a capacitance which collects the charge of an incoming pulse. The voltage at this anode capacitance increases instantly as the charge impinges, i.e. if a charge Q impinges onto the anode the voltage U_{Anode} is produced:

$$U_{Anode} = \frac{Q}{C_{Anode}} \quad (2.1)$$

The voltage U_{Anode} is also the input voltage U_e of the operational amplifier. The operational amplifier of the entrance stage is wired as integrator with a feedback capacitance C_R (resistor R_R will be neglected at first). As explained previously the operational amplifiers will adjust their output such that the voltage difference between the two inputs is zero. As the non-inverting input is connected to ground the voltage at the inverting input must be also 0 V. If a charge Q impinges onto the anode, a voltage step U_a must occur at the output which compensates the anode charge:

$$U_a = -\frac{Q}{C_R} \quad (2.2)$$

Simply explained it is such, that the charge Q is transferred from the anode capacitance C_{Anode} to the feedback capacitance C_R .

Exercise 5:

Estimate from Eq. (2.2) the formula for the charge amplification of the entrance stage (1. operational amplifier) of the charge amplifier shown in Fig. 2.22 in [Volt/Coulomb]. Calculate the output voltage of this integrator stage for a feedback capacitance $C_R = 3 \text{ pF}$ and an impinging charge of 10^7 electrons.

The entrance stage is named integrator, as the output voltage is proportional to the time integral of the incoming current. In other words, the output voltage is proportional to the sum of the incoming charges. Without further measures the output voltage would increase until it is clipped by the supply voltage (Fig. 2.23). To avoid this, the feedback capacitance must be discharged slowly to bring the output voltage back to 0 V. This is the task of the feedback resistor R_R . R_R has to be chosen large enough, that U_a will not

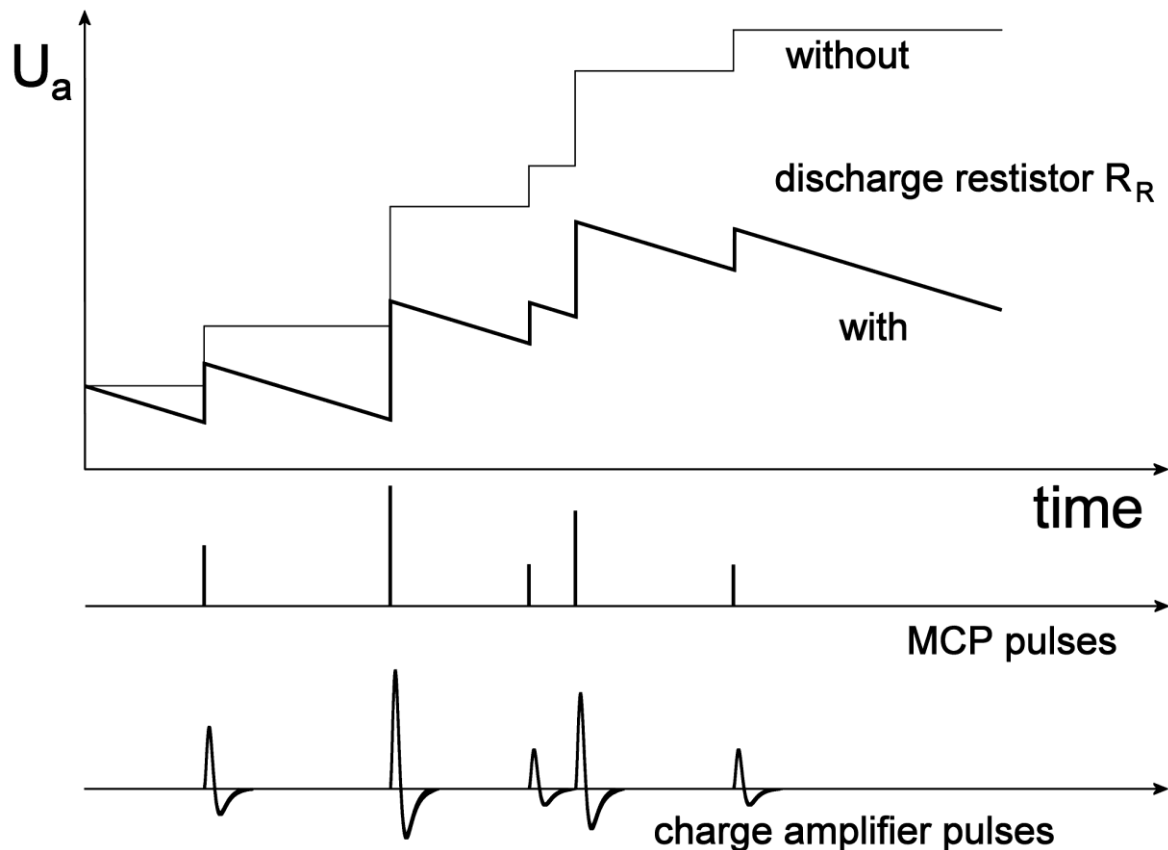


Fig. 2.23

Principle of charge amplification: At the output of the integrator stage the incoming MCP pulses produce a voltage U_a which rises in steps for each pulse. Without feedback resistor R_R , which discharges the capacitor C_R , the output would result in an ever increasing voltage until the maximum voltage would be achieved. With discharge resistor the output voltage results in a saw tooth like course (the linear decline is the beginning of an exponential discharge curve). The information about the amount of charge is stored in the voltage steps. To be able to process this information in a more simple way, a filter stage is added to the charge amplifiers, which produce the bipolar pulses shown at the bottom (see also Fig. 2.25). The amounts of charge can now be evaluated from the peak voltages of the bipolar pulses.

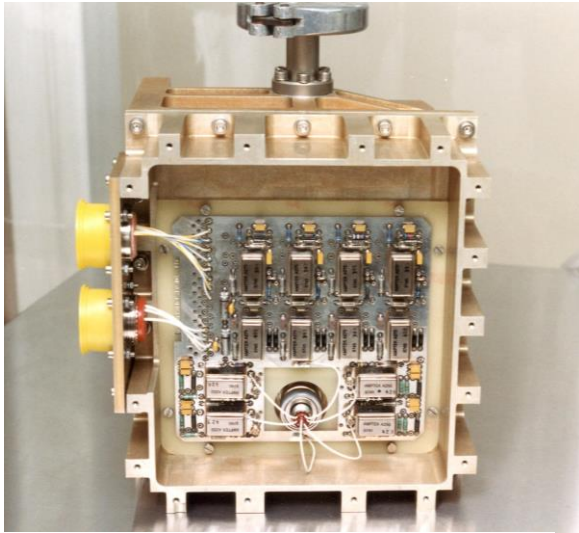


Fig. 2.24
View of the charge amplifiers of the ORFEUS detector

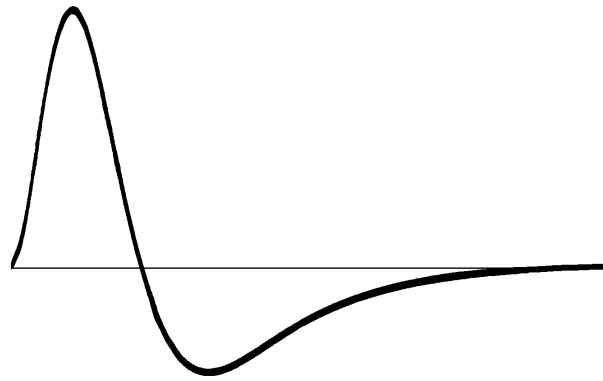


Fig. 2.25
Form of the output pulse after the filter stage:
Maximum at 1.1 μs , zero crossing at 2.3 μs . Time span shown: 10 μs .

change within the time span that the electronics needs to register a pulse. On the other hand R_R has to be chosen small enough that the output voltage U_a will not be clipped at the highest expected pulse rates. The timing course of the output voltage U_a is such that a voltage step occurs at each impinging charge pulse which is followed by an exponential decay. The voltage will not drop to 0 V until the next pulse occurs, depending on the time when the next pulse arrives.

The information needed for registering one pulse is contained in the voltage step, i.e. in an extremely short change at the output of the integrator stage. Such a voltage step within an otherwise exponential decaying course cannot be registered with further measures. Therefore a final filter stage is needed which forms the voltage step into a well-defined voltage pulse (Fig. 2.25). These pulses have the advantage to show a pronounced maximum (proportional to the height of the voltage step) and to achieve a stable zero level again within a few microseconds. As the pulses are bipolar with the same areas enclosed by the positive and negative part, these pulses can be transmitted capacitively without shifting the zero level when the count rate changes. The capacitive coupling is important, when the pulses are to be transmitted over longer distances. The DC part could be shifted when the signal is transmitted over long cables, if the resistances in the power supply cables cannot be neglected.

2.4.3 Digital Position Analyzer

The detector transmits four bipolar voltage pulses to the analyser electronics for further evaluation of the event. The flight electronics of the ORFEUS mission comprised this analyser electronics which determined the position of each event, as well as the onboard computer for data acquisition. Both, the analyser electronics and the on-board computer system were developed and built by our institute. In Fig. 1.1 the cover of this electronics can be seen as black rectangle below the Echelle Spectrometer, which protrudes from the telescope.

Our current experiment makes use of an analyser electronics which was built originally for an optical detector: The Digital Position Analyzer (DPA). This electronics performs the following tasks:

- Recognition of pulses
- Digitising of the maximum values of the voltage pulses (X_1, X_2, Y_1, Y_2) with a resolution of 12 bit
- Calculation of the sums $\sum X_i, \sum Y_i$
- Calculation of the positions $\mathbf{X} = X_2 / \sum X_i, \mathbf{Y} = Y_2 / \sum Y_i$ with a resolution of 12 bit
- Calculation of the pulse height
 $Z = \sum X_i + \sum Y_i$
- Acquisition of the time for each event
- Transmission of the data to the computer

The pulse processing is controlled by an electronic control circuitry, which uses as input the sum of the four charge amplifier signals. The most important task is to determine the maxima of the pulses which have to be digitised. Therefore the signal is split into an attenuated (grey, Fig. 2.26) and a delayed (black) part. Both parts are fed into the two inputs of a comparator. With a potentiometer the attenuation is adjusted such that the delayed pulse crosses the attenuated pulse exactly in

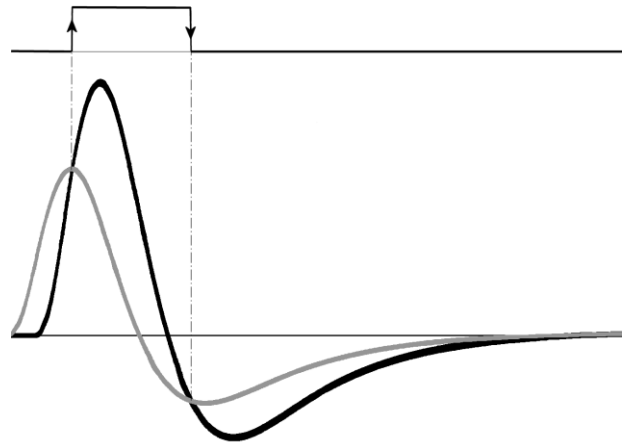


Fig. 2.26
Determination of the maximum of the signals: attenuated summed pulse (gray) and delayed summed pulse (black) are fed into the two inputs of a comparator. The upper curve shows the output signal of the comparator.

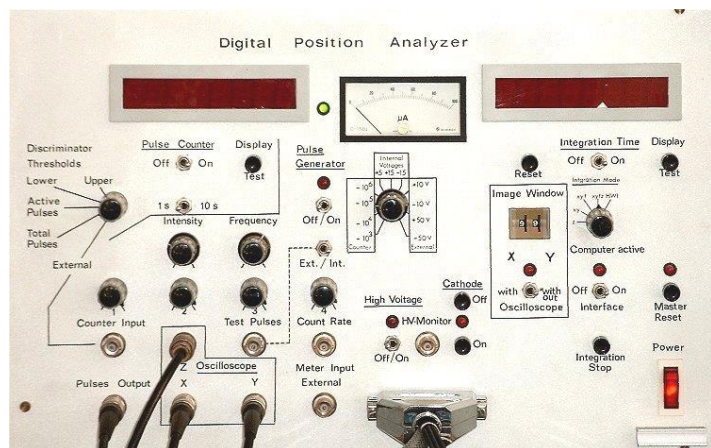


Fig. 2.27
Front view of the DPA

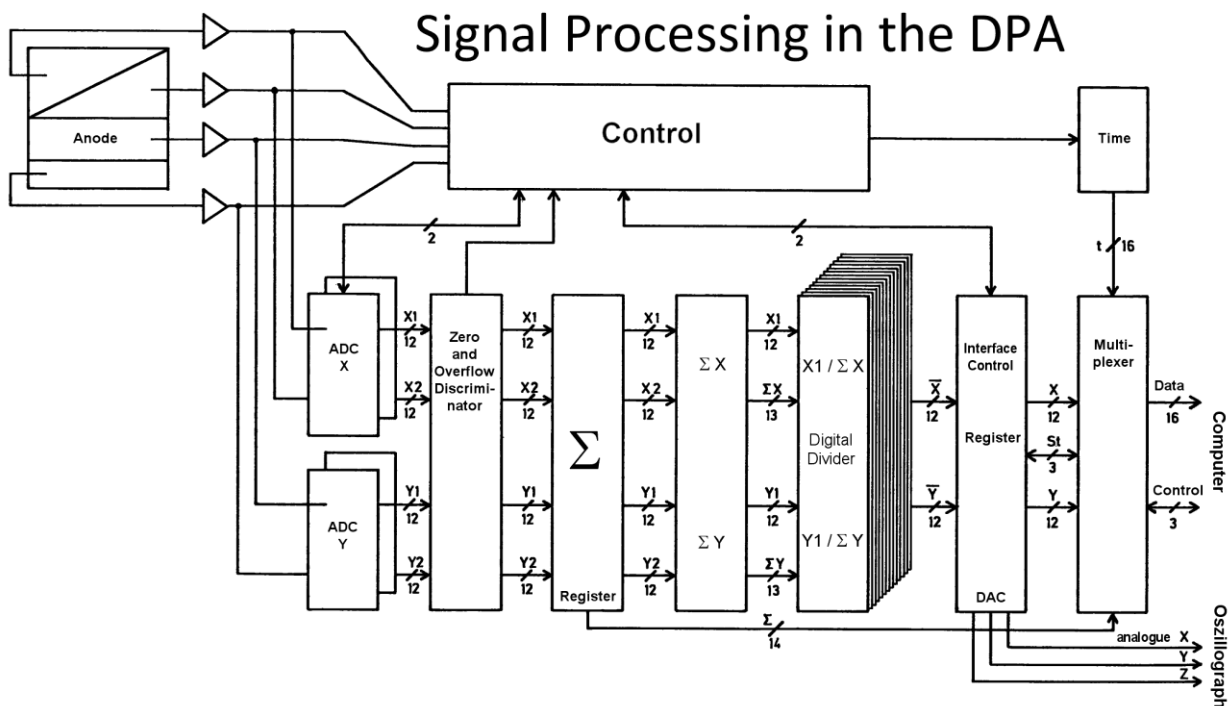


Fig. 2.28
Block diagram of the DPA (source: Barnstedt 1985)

its maximum, causing the comparator to produce a rising edge. This triggers the analogue to digital converters which hold the maximum values of the four signals and digitise them. This approach has the advantage, that the estimation of the maximum functions independently of the actual pulse height. Two further comparators allow the adjustment of a lower and an upper discriminator threshold, which inhibit the acceptance of pulses which are too weak or which are overloaded. Fig. 2.27 shows the front view of the DPA; a block diagram is shown in Fig. 2.28. A separate manual exists for the DPA.

2.4.4 Data acquisition with the computer

For data acquisition a PC with a Windows operating system is used. This computer comprises 2 interfaces: one multi-purpose interface with analogue and digital inputs and outputs for controlling of the detector and the high voltage supply and one fast 32 bit parallel interface for the acquisition of the detector data. Software exists which allows to control the high voltage and the test pulses as well as software for data acquisition. Data acquisition may be run in several modes:

- Image integration (X, Y): Recording of the coordinates with 10 bit (image size 1024 x 1024 pixels)
- Integration of a pulse height distribution (Z)
- Integration of an image and of a gain map (X, Y, Z)
- Serial recording of all events including time information for each photon with microsecond time resolution (X, Y, Z, T)

Separate manuals exist for these programs.

2.5 Characteristics of the detector electronics

This chapter deals with those imaging characteristics of the detector system that are caused by the electronics. These comprise the noise of the charge amplifiers, unequal amplification factors of the four charge amplifiers and capacitive cross talk between the four anode electrodes.

2.5.1 Noise

As the position of a photon is calculated for each axis from two charge amplifier signals, the noise of these signals has direct influence on the position resolution of the detector. The noise may be described by a Gaussian distribution of the measured voltage around a mean value with a standard deviation (mean squared error) σ_U . If a value x is calculated from the voltages U_1 and U_2 as $x = U_1/(U_1+U_2)$ at which the voltages U_1 and U_2 are superposed by a noise with standard deviation σ_U , it can be shown (Knapp 1978) that x also is Gaussian distributed around a mean value. The standard deviation of x is calculated as

$$\sigma_x = \frac{\sigma_U}{z} \sqrt{2x^2 - 2x + 1} \quad (2.3)$$

with $z = U_1+U_2$. The expression $\sqrt{2x^2 - 2x + 1}$ becomes unity for $x = 0$ and $x = 1$ (i.e. at the anode border), while for $x = 0.5$ (i.e. in middle of the anode) a minimum with a value of $1/\sqrt{2} = 0,71$ is achieved. The distribution in X direction corresponds to a cut through an image of a point source (point spread function). For a description of the resolution it is better to use the full width at half maximum (*FWHM*) than the standard deviation σ :

$$FWHM = \sigma \cdot 2\sqrt{2 \cdot \ln 2} = 2,35 \cdot \sigma \quad (2.4)$$

The *FWHM* can be regarded as resolution limit, i.e. the smallest distance at which two point images still could be distinguished. The resolution in line pairs per length unit is thus calculated as $1/FWHM$.

2.5.2 Partition Noise

The electron cloud impinging onto the anode comprises a finite number of electrons. These electrons are distributed onto the four electrodes. This partitioning results in statistical fluctuations of the number of electrons that arrive at each of the four electrodes. These fluctuations are called Partition Noise. Which influences have such fluctuations on the accuracy of the calculated position?

To simplify matters it could be assumed that the position encoding in the two axes is independent of each other. The two wedge electrodes or the two strip electrodes each obtain half of the total charge arriving at the anode. Let's have a look at the wedge electrodes which encode the x direction. At position x (normalised, $0 \leq x \leq 1$) a charge cloud with a total charge Q impinges onto the anode. Both wedges together obtain the charge $Q/2$ and the number of electrons $N/2$ with $N = Q/q$ and $q =$ electron charge. In the average wedge electrode 1 will get $N_1 = x \cdot N/2$ electrons and wedge electrode 2 will get $N_2 = (1-x) \cdot N/2$ electrons.

Statistically each of the $N/2$ electrons will hit electrode 1 with probability $p_1 = x$ and electrode 2 with probability $p_2 = 1-x$. Such a situation, in which one event may achieve one of two states, is statistically described by a binomial distribution (Weinzierl / Drosig 1970):

$$P_{n,p}(k) = \binom{n}{k} \cdot p^k \cdot (1-p)^{n-k} \quad (2.5)$$

The distribution $P_{n,p}(k)$ describes the probability, that after n trials exactly k positive events are registered, if the probability for a positive event is p . In our case the number of trials is $n = N/2$, i.e. the number of electrons impinging onto the wedge electrodes. A positive event is the arrival of an electron at electrode 1, thus $p = p_1 = x$, and k is the number of electrons that were collected by electrode 1.

For the standard deviation σ of the values k around the average N_1 the following equation is valid for a binomial distribution:

$$\sigma = \sqrt{p \cdot (1-p) \cdot n} = \sqrt{x \cdot (1-x) \cdot \frac{N}{2}} \quad (2.6)$$

The left square root shows the general case and the right square root is valid in our case with the definitions given above.

σ becomes zero at the borders of the anode ($x = 0$ and $x = 1$), while it becomes maximal at the centre ($x = 0,5$): $\sigma_{\max} = 0,5 \cdot \sqrt{N/2}$. This value refers to the actual number of electrons. To calculate the variance of a relative position x ($0 \leq x \leq 1$), this value has to be divided by the number of electrons $N/2$. Additionally we use Eq. (2.4), to convert the standard deviation approximately into a *FWHM*. Thus the following equation is valid for the *FWHM* of a point image in the centre of the anode which is broadened by partition noise:

$$FWHM_{part} = 2,35 \cdot \frac{1}{\sqrt{2N}} = 1,66 \cdot \frac{1}{\sqrt{N}} \quad (2.7)$$

The inverse of this value is a measure for the number of image points that can be distinguished in one axis. This gives the following numbers: for $N = 10^6$: 600, for $N = 10^7$: 1900 and for $N = 10^8$: 6000. Thus partition noise does not play a significant role for a detector with 1024 pixels per axis, if we have more than about 10^7 electrons per electron cloud.

2.5.3 Cross talk

The electrodes act as capacitances against each other. The charge amplifiers have a dynamic input capacitance. Corresponding to the ratio of input capacitance to electrode capacitance, a part of the charges impinging onto the electrodes will couple capacitively onto the other electrodes (cross talk). How affects this the calculated position x ?

Let us consider first the ideal coordinate in one axis, for example the X axis, which is calculated from the two wedge charges Q_1 and Q_2 (the total charge is $Q = Q_1 + Q_2$):

$$x = \frac{Q_2}{Q_1 + Q_2} = \frac{Q_2}{Q} \quad (2.8)$$

x may receive values from 0 (= left anode border) to 1 (= right anode border). The measured voltages U_1 and U_2 are calculated with the amplification factor v and a cross talk fraction b as $U_1 = v \cdot (Q_1 + bQ_2)$ and $U_2 = v \cdot (Q_2 + bQ_1)$. Thus we get for x' :

$$x' = \frac{U_2}{U_1 + U_2} = \frac{Q_2 + bQ_1}{Q_1 + bQ_2 + Q_2 + bQ_1} \quad (2.9)$$

If equation (2.8) is resolved for Q_2 and inserted again into (2.9), Q will cancel down and the following relation between the measured position x' and the real position x is obtained:

$$x' = \frac{x(1-b) + b}{1+b} = x \frac{1-b}{1+b} + \frac{b}{1+b} \quad (2.10)$$

Consideration of plausibility:

$x = 0:$	$x' = b/(1+b)$
$x = 1/2:$	$x' = 1/2$
$x = 1:$	$x' = 1-b/(1+b)$

Thus the cross talk causes the registered image to shrink, as both borders are shifted towards the centre by the amount $b/(1+b)$.

2.5.4 Amplification differences

To achieve an exact linear imaging it is necessary that the two charge amplifiers, whose signals are used to calculate the position in the respective axis, have exactly the same amplification (and also the same temporal behaviour). This means, that all electronic components of the circuitry shown in Fig. 2.22 have exactly the same values. As electronic components always have a certain tolerance with respect to their nominal value, it is necessary to measure the individual values of many components and use the best matching ones at the same positions of the two charge amplifiers. With electronics used in the laboratory it is possible to adjust resistors with potentiometers. This is also possible with capacitors by using special trim capacitances. But this possibility does not exist for electronics which is to be used in space applications, as potentiometers are not shock proof. You have to use one or two additional adjustment resistors which are fixed after soldering them into the circuitry. This usually achieves accuracies only in the percentage range. Therefore one has to deal with the fact, that the amplification factors are identical only within a few percent. This leads to nonlinearities in the imaging which have to be considered during data reduction.

What is the formula for this nonlinearity? The real position x is defined in equation (2.8). Ideal charge amplifiers produce voltage pulses U_1 and U_2 which are exactly proportional to Q_1 and Q_2 . But in practice

the two amplification factors will be slightly different. We thus assume $U_1 = v \cdot Q_1$ and $U_2 = v \cdot (1+a) \cdot Q_2$; a is a small corrections value for the amplification factor which might be also negative. The electronics calculates actually the position x'' :

$$x'' = \frac{U_2}{U_1 + U_2} = \frac{Q_2(1+a)}{Q_1 + Q_2(1+a)} \quad (2.11)$$

If equation (2.8) is resolved for Q_2 and inserted again into (2.11), Q will cancel down and the following relation between the measured position x'' and the real position x is obtained:

$$x'' = x \frac{1+a}{1+xa} \quad (2.12)$$

Check for plausibility: For $a = 0$ the identity $x'' = x$ is obtained. In all other cases the values for the borders remain unchanged: $x = 0$ results in $x'' = 0$ and $x = 1$ obtains $x'' = 1$. Thus the image is distorted such that the image borders remain unchanged but the centre of the image is somewhat shifted.

Like cross talk this effect too has to be corrected at the stage of data reduction. It has to be considered, that cross talk occurs before the different amplification factors go into the calculation of the position.

Calculating the derivative of x'' with respect to x , one will get a measure for the number of pixels per length unit at anode position x (if x'' is given in pixels and x in real anode size):

$$\frac{dx''}{dx} = \frac{1+a}{(1+xa)^2} \quad (2.13)$$

The reciprocal value would be a measure for the pixel size at the anode position x . A value of 1 corresponds to the nominal value, which one for example also gets with $a = 0$. There always exists an x -position with a derivative of 1, as at both borders one value is larger and the other smaller than 1.

Setting $\frac{dx''}{dx} = 1$ and resolving for x , one obtains:

$$x = \frac{\sqrt{1+a} - 1}{a} \approx \frac{1}{2} - \frac{1}{8}a \quad (2.14)$$

The last term results after series expansion of the square root up to the quadratic term. As expected the nominal pixel size is obtained near the centre of the image.

Exercise 6:

Derive equation (2.13) from equation (2.12).

2.5.5 Offset

As described in chapter 2.4.1 (p. 20), the pulses of the charge amplifiers may be capacitively transmitted without any shift in the zero level of the signal lines. But such shifts of the zero level may occur in the further course of the signal processing, especially with the analogue-to-digital converters (ADC). These shifts are called offset voltages. Therefore each ADC circuitry of the DPA comprises a potentiometer, which allows adjusting the offset voltage to zero.

How is such an offset error visible in the image? Assume a constant offset voltage on the second signal, which would correspond to an offset charge Q_{off} . With $U_1 = v \cdot Q_1$ and $U_2 = v \cdot (Q_2 + Q_{\text{off}})$ one obtains for the calculated position x''' :

$$x''' = \frac{U_2}{U_1 + U_2} = \frac{Q_2 + Q_{\text{off}}}{Q_1 + Q_2 + Q_{\text{off}}} \quad (2.15)$$

With the same definitions of x and Q as in the previous chapters this can be converted into

$$x''' = x \frac{1}{1 + \frac{Q_{\text{off}}}{Q}} + \frac{Q_{\text{off}}}{Q + Q_{\text{off}}} \quad (2.16)$$

Assuming that $Q_{\text{off}} \ll Q$, the first fraction can be expanded to the first order in a series and in the second fraction Q_{off} could be neglected against Q :

$$x''' \approx x \left(1 - \frac{Q_{\text{off}}}{Q} \right) + \frac{Q_{\text{off}}}{Q} \quad (2.17)$$

Considering the borders:

$$\begin{aligned} x = 0: & \quad x''' = Q_{\text{off}} / Q \\ x = 1: & \quad x''' = 1 \end{aligned}$$

While no change is seen at the right border ($x = 1$), the left border ($x = 0$) is shifted by Q_{off} / Q . The shift therefore also depends on the total charge and is largest for small pulses. This shift occurs at that border, at which the signal affected by the offset error (Q_2 in this example) is small, as the relative error Q_{off} / Q_2 is particularly large.

2.5.6 Dead time

The electronic effect of dead time affects the efficiency of the detector. Dead time means those time spans during which the electronics is not able to process arriving pulses. The reason could be that the electronics is busy with processing of a pulse (e.g. AD conversion), or that a measurement would be distorted (e.g. during the settling of a pulse, see Fig. 2.25).

The DPA processes an AD conversion within 2 μs , which is much faster than the settling of the charge amplifier pulses. Also the digital calculation of the position is quite fast with about 0.5 μs . Thus the charge amplifier pulses are the slowest element in the signal processing chain, as they need about 10 – 13 μs for settling. Only after complete settling to 0 V a new pulse can be processed again, as otherwise the signal would be distorted by an offset error.

To inhibit the signal processing during the settling of a charge amplifier signal the control logic of the DPA uses a monoflop which is triggered by the zero crossing of the pulses at about 2 μs . It inhibits the pulse recognition for about 11 μs . Pulses which arrive during this time will retrigger the monoflop, i.e. the active state of the monoflop is lengthened again by 11 μs . In total the dead time of one pulse is about 13 μs .

Pulses that arrive within one microsecond (up to the maximum of the first pulse) cannot be distinguished by the electronics. Such nearly coincidental pulses are processed as one pulse. This effect is called pile-up. Most of these pile-up pulses are large enough to trigger the upper discriminator threshold and are therefore suppressed.

Which influence has the dead time on the electronic efficiency of the system? The registered events of our detector are statistically independent of each other; they therefore can be described by a Poisson distribution (Weinzierl / Drosig 1970):

$$P_x = \frac{m^x e^{-m}}{x!} \quad (2.18)$$

This gives the probability to observe x positive events, if the mean value of this probability distribution is m . In our case positive events are the number of pulses occurring during the observation time t . With a mean count rate n_0 , m is calculated as $m = n_0 \cdot t$. The probability that no event occurs during the measuring time t is therefore (with $0! = 1$):

$$P_0 = e^{-n_0 t} \quad (2.19)$$

The probability that one pulse is observed in the following time interval between t and $t + dt$ is exactly $n_0 \cdot dt$ (by definition of n_0 and with $dt \ll 1/n_0$). As the probabilities are independent of each other, they can be multiplied to obtain the probability, that exactly one event occurs after the time t in the time interval dt :

$$dP_t = n_0 \cdot e^{-n_0 t} dt = e^{-n_0 t} d(n_0 t) \quad (2.20)$$

Therefore short time intervals between the registered pulses are exponentially more frequent. It is therefore principally impossible to obtain lossless measurements with an electronics that has a dead time. Thus pulses are registered by electronics with dead time τ only, if their interval to the previous pulse is larger than τ . By integration of equation (2.20) one obtains for the probability of pulse intervals $t > \tau$:

$$P_{t>\tau} = \int_{t=\tau}^{\infty} dP_t = n_0 \int_{\tau}^{\infty} e^{-n_0 t} dt = e^{-n_0 \tau} \quad (2.21)$$

As the mean pulses n_0 arriving per time unit are statistically independent, the number of events n registered by the electronics is given by

$$n = n_0 \cdot e^{-n_0 \tau} \quad (2.22)$$

For very large count rates ($n_0 \rightarrow \infty$) n tends to zero, i.e. practical all pulse intervals are smaller than the dead time τ . Therefore a maximum exists for the curve defined by equation (2.22). By differentiation of (2.22) with respect to n_0 and subsequent root-finding, the maximum is found at $n_0 = 1/\tau$ and thus the maximum number of events that can be registered are

$$n_{\max} = \frac{1}{\tau \cdot e} \quad (2.23)$$

With $\tau = 13 \mu\text{s}$ one obtains for the maximum rate of registered events $n_{\max} = 28.300 \text{ s}^{-1}$ at an incoming rate of $n_0 = 76.900 \text{ s}^{-1}$; the efficiency is $1/e = 37 \%$ (Fig. 2.29).

To estimate the real incoming rate n_0 from a measured rate n with known dead time τ usually the

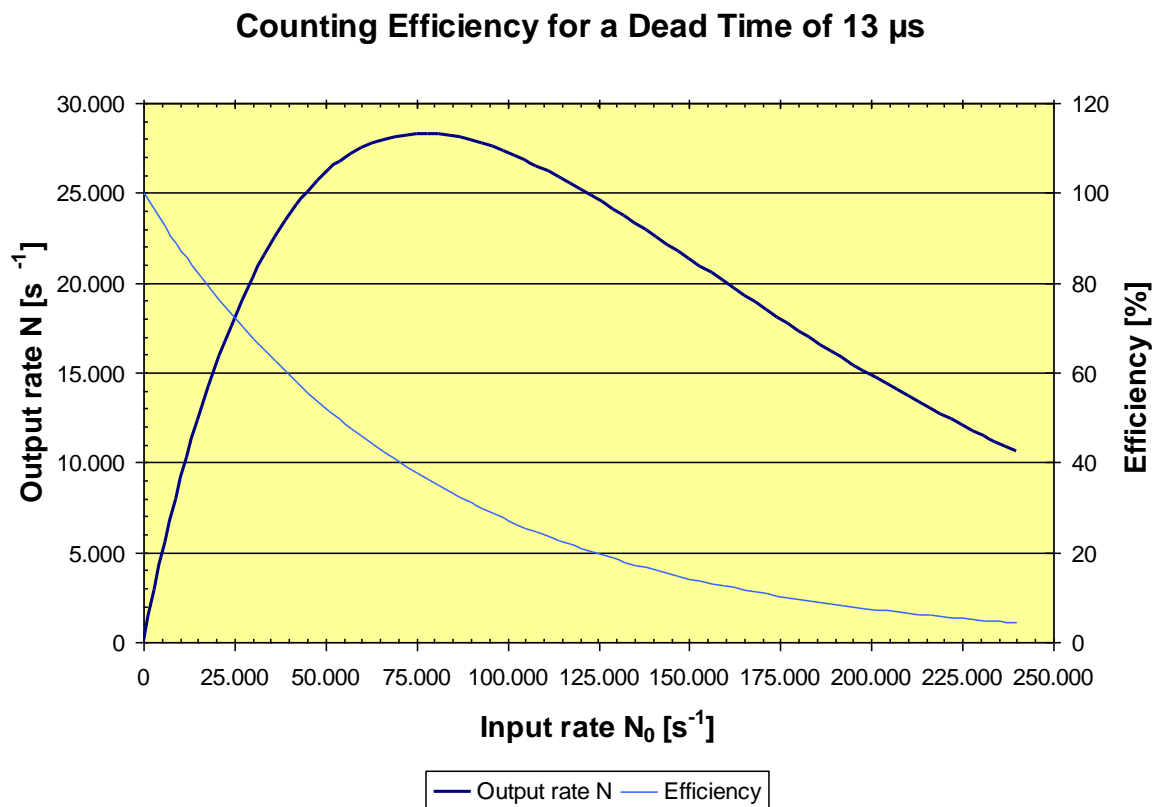


Fig. 2.29

Output rate and efficiency for a dead time of $\tau = 13 \mu\text{s}$ in relation to the input rate

following approximation is used, as equation (2.22) cannot be analytically resolved for n_0 :

$$n_0 \approx \frac{n}{1 - n \cdot \tau} \quad (2.24)$$

This approximation obviously can be used only at count rates that are significantly smaller than $1/\tau$. If $n_0 < 14\%$ of $1/\tau$ ($n < 12\%$), then the error made with this formula is smaller than 1%, with $n_0 = 44\%$ of $1/\tau$ ($n = 28\%$) the error is already 10%.

A more accurate approximation can be derived, if in equation (2.22) the exponential function is expanded in a series. Considering in this series expansion the summands up to the quadratic term and resolving the equation for n_0 , one obtains after longer calculation:

$$x_0 \approx \frac{1}{3} \left(2 + \sqrt[3]{x' + \sqrt{x'^2 + 8}} + \sqrt[3]{x' - \sqrt{x'^2 + 8}} \right) \quad (2.25)$$

The following definitions apply: $x' = (27x - 10)$; x and x_0 are normalised count rates: $x = n \tau$ and $x_0 = n_0 \tau$. If $n_0 < 0,33/\tau$ ($n < 0,24/\tau$) this correction gives an error of less than 1% and with $n_0 < 0,62/\tau$ ($n < 0,33/\tau$) the error is less than 10%. With both given formulas the calculated value of n_0 is smaller than the real value.

For the sake of completeness it should be noted, that electronics with other dead time characteristics exist also. Such electronics can process a new event immediately after the end of the dead time, irrespective of the number of pulses that arrived during the dead time. An example would be a detector system with very short analogue pulses which could be neglected against the time span needed for AD conversion. Pulses arriving during AD conversion would not interfere with it (the analogue voltage to be digitised is usually stored in a sample-and-hold circuitry). The pulses arriving in this time span would be ignored, but immediately after AD conversion a new pulse could be processed. With this dead time characteristic the maximum achievable output rate tends towards a constant value of $n_{\max} = 1/\tau$.

In our *ORFEUS* detector however the analogue pulses are the slowest element of the signal processing chain. Therefore an optimisation of the detector electronics in future projects should aim in using much faster charge amplifiers.

3 Experimental setup

The experimental setup comprises four components:

- Detector with high voltage supply and vacuum pump
- Optical bench
- Rack with DPA, storage screen, pressure gauge and oscillograph
- Computer

3.1 *Detector with high voltage supply and vacuum pump*

Fig. 3.1 shows the detector with high voltage supply. On the left is a vacuum connection which leads to the vacuum pump. The vacuum valve mounted at the detector always must be fully opened, i.e. the actuation screw of this valve must be completely unscrewed. **This has definitely to be checked before switching on the high voltage!**

As the pumping down of the detector takes quite a long time, the vacuum pump should be running all the time and the detector thus should be kept always under vacuum.

If the vacuum pump has to be switched off, the complete vacuum system has to be filled with Argon. The detector valve has not to be closed until a slight over pressure is achieved. This prevents the detector to be filled by air through small micro leaks which are always present in vacuum systems. The humidity of air would destroy the KBr photo cathode by and by. Under a pure Argon atmosphere the detector can be stored without any change in the detector characteristics.

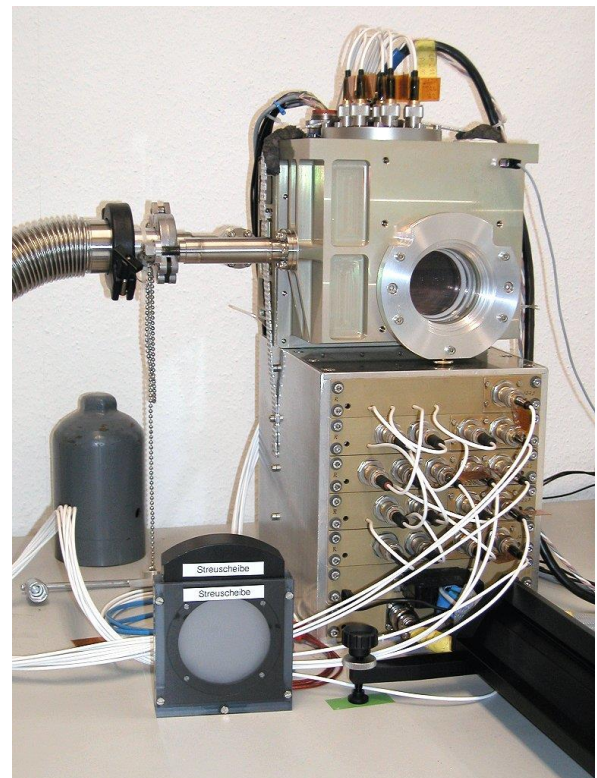


Fig. 3.1
Detector with high voltage supply and diffusion disc

The pressure gauge mounted in the rack measures the pressure directly at the pump. The pressure is shown in millibars (= hPa). The pressure inside the detector housing is about a factor 100 worse, as the pumping cross-section through the flexible tube and the valve is very small. If the detector is not in operation, the pressure reading is about $5 \cdot 10^{-7}$ mbar. The high voltage may be switched on only if the pressure reading is below $1 \cdot 10^{-6}$ mbar.

When the detector is switched on, the pressure will rise. The reason is that all surfaces under vacuum will adsorb molecules of the residual gases and so do also the surfaces of the channels of the MCPs. If these surfaces are bombarded by electrons the gas molecules will be released and the surfaces are cleaned by this process. This outgassing leads to an increased pressure until the walls are clean.

Exercise 7:

Calculate the total surface of all channels of an ORFEUS MCP which has a thickness of 1 mm (see Chap. 2.2.7, p. 13).

3.2 Optical bench

The optical bench (Fig. 3.2) comprises the following optical components:

- Mercury lamp: The lamp emits an emission line at 254 nm, for which the detector is sufficiently sensitive. In front of the lamp an UV diffusion disc is mounted, which assures a homogeneous angular distribution of the emitted light.
- Small iris diaphragm
- Quartz condenser lens: By variation of the distance of the condenser lens to the lamp the light intensity falling onto the detector can be adjusted.
- Resolution test mask
- Quartz lens with large iris diaphragm: The lens has a focal length of 20 cm (for visible light).
- Mask support with further test masks

Not all components are needed all the time on the optical bench.



Fig. 3.2
Optical bench with all components (from back to front): lamp, small iris diaphragm, lens with large diaphragm, test mask, condenser lens.

Exercise 8:

What is the smallest possible distance between test mask and detector, which still allows imaging with the given lens? Which reproduction scale is achieved? Why are the lenses used in this experiment made from quartz?

Note:

UV light may be irritating to the eyes; therefore it should be avoided to look into the light source for longer time, although the light intensity is very low. This is valid especially when the lamp is operated without the diffusion disc (spectacle wearers may ignore this hint). To avoid sunburn, you also should not expose unprotected parts of your skin (hands) directly in front of the lamp for longer time. The lamp has to be switched off if not needed.

3.3 Digital Position Analyzer

The Digital Position Analyzer (DPA) comprises all important operating controls needed for the detector electronics (see also Chap. 2.4.3, p. 23). These are (Fig. 3.3):

- Pulse counter with selection of counting time (1 s / 10 s).
- Selection switch for the pulses to be counted:

- **Total Pulses:** counts all pulses; the trigger threshold is adjusted to a positive value which lies just above the noise level.

- **Active Pulses:** counts only pulses, which are processed by the electronics. During integration this are only those pulses, which are transferred to the computer.

- **Lower Discriminator Threshold:** counts all pulses which trigger the lower discriminator threshold of the electronics.

- **Upper Discriminator Threshold:** counts all pulses which trigger the upper discriminator threshold of the electronics.

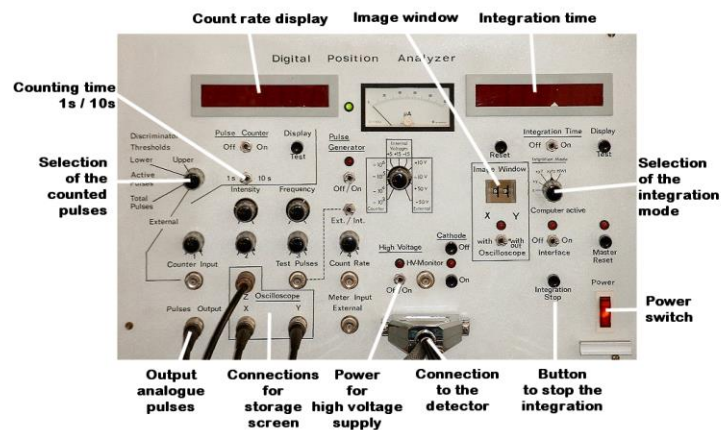


Fig. 3.3
Some important operating controls of the DPA (see also Fig. 2.27).

- Output of the analogue pulses for connection of an oscillograph
- 3 connections for a storage screen for real-time display of the registered events
- Power switch for the high voltage supply unit
- Connector for detector cable
- Switch to stop the integration
- Power switch
- Selection switch for integration modes:
 - Position 1 (**Z**): Only the sum of the pulse heights **Z** is transmitted to integrate a pulse height distribution.
 - Position 2 (**X, Y**): The position coordinates are transmitted to integrate an image.
 - Position 3 (**X, Y, T**): The position coordinates and the time are transmitted for serial recording of the data. A later data reduction may reconstruct the timing behaviour.
 - Position 4 (**X, Y, T, Z**): Transmission of all data which allows all kinds of integration. In particular only in this position an integration of a gain map of the detector is possible.
 - Position 5 (**HWI**) has no function in the current configuration.
- Display of the integration time: The time is shown in milliseconds; a mark shows the decimal point for seconds. The time displayed is corrected for dead time, i.e. the internal clock is only running, if the electronics is ready to process new events.
- Selection switch for image window: This switch enables the selection of a partial image from a 4x4 matrix. These partial images are recorded with 12 bit resolution, but the size of the recorded images is also 1024 x 1024 pixels. Valid values for X and Y range from 0 ... 3.

A separate manual for the DPA is available.

3.4 Storage screen

The storage screen (Fig. 3.4) shows the real time detector image. Each registered event is shown as light dot via X/Y control on the screen. Two modes are available: Normal mode (button *STORE* not pressed) and storage mode (button *STORE* pressed):

- Normal mode: Each event produces a short flashing light dot which is not stored. This mode is usable for fast varying images at high count rates. Usually the beam intensity has to be increased in this mode (turning knob *INTENSITY* behind the cover).
- Storage mode: Each short flashing dot is stored for a certain time. The persistence can be adjusted with the turning knob *PERSISTENCE*. When this knob is pulled the current image remains stored. The turning knob *OPERATE LEVEL* adjusts the brightness of the stored image. The button *ERASE* erases the stored image.

As this storage screen has a limited life time it should not be operated longer as necessary in storage mode. When the beam stands still the intensity should be lowered to avoid burning in of the beam spot.

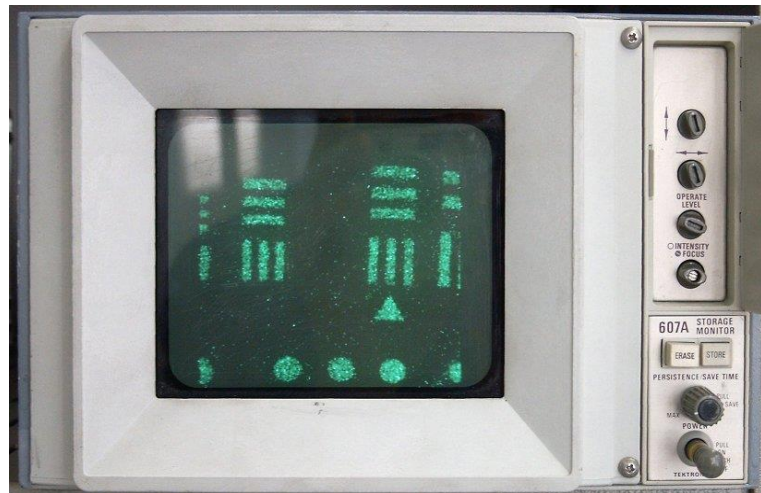


Fig. 3.4
Storage screen with real time detector image.

3.5 Oscilloscope

The oscilloscope (Fig. 3.5) displays the summed pulses of the detector. The best settings are:

- Y-Amplification: 1 V/DIV
- Time base: 0.5 μ s/DIV
- Trigger: small positive voltage, rising edge

When test pulses are displayed also inverted pulses are visible, as test pulses are produced by square pulses, which have a rising and a falling edge and only the falling edge simulates normal electron clouds on the anode. The inverted pulses are triggered during the (positive) zero crossing of the undershoot, resulting in two different pulse forms visible on the oscilloscope screen.

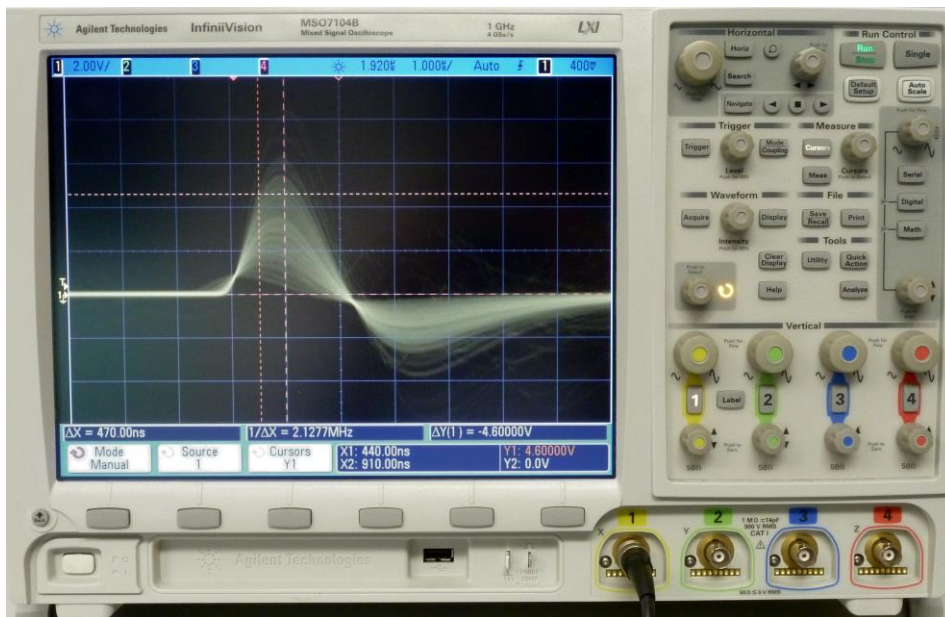


Fig. 3.5
Oscillograph with detector pulses.

3.6 Computer and software

Two programs are needed for the operation of the detector and for data acquisition. Program “*HV-Control*” controls the high voltage of the detector and also allows for different testing methods with test pulses. Program “*Aquisition*” is needed for data acquisition and allows for the integration of the events registered by the detector. Both of these programs are shortly introduced here, a detailed manual is separately available.

3.6.1 Program *HV-Kontrolle*

The program “*HV-Control*” is primarily needed for control and monitoring of the high voltage supply of the detector. It also monitors the pressure of the vacuum system and shuts down the high voltage or inhibits its switching on if a pressure threshold is exceeded. The most important functions and displays will be described in the following. The program setup (menu “*Einstellungen*”) is usually not changed during the practical course (except for changing the update rate of the protocol) and changes should therefore only be done by the assistant. All measured values are regularly written into a protocol file, the update rate may be adjusted to the current needs.

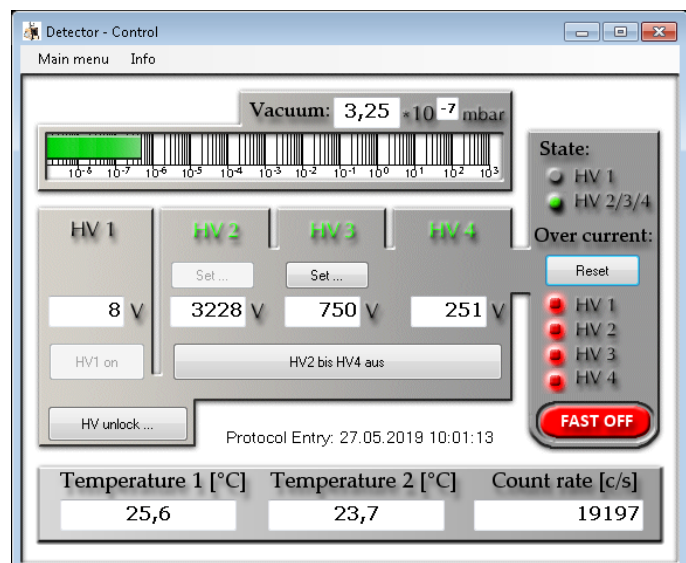


Fig. 3.6
Main window of the program *HV-Control*.

3.6.1.1 Main window

The main window shows the pressure of the vacuum system, the four measured voltages of the high voltage supply of the detector and the detection of an over current in one of the four high voltage modules. Also two temperature values are shown (outside of the detector housing and at the charge amplifiers) as well as the current pulse count rate and time and date of the last protocol entry.

The high voltage is switched on by clicking the buttons labelled “*HV1 an*” and “*HV2 to HV4 on*”. Before these buttons can be clicked, they have to be unlocked by clicking the button labelled “*HV Entsichern...*”. You then have to confirm that the vacuum valve of the detector is opened (only then the measured pressure is valid also for the detector) by selecting the option “*Das Vakuum-Ventil ist offen!*”. After confirming this, the buttons for switching on the high voltage are active (enabled) for 5 seconds. Only during this time it is possible to switch on the high voltage. This prevents an unintended switching-on, which might have possibly catastrophic consequences.

3.6.1.2 Test pulses

The menu item “*Test Pulses*” switches on the test pulses (see Chap. 2.3.4, p. 17). It is possible to change the pulse frequency, the rate at which the different pulse types are switched, and the selection of the 6 possible pulse types. The selected pulse types are switched on in sequence with the given rate, as only one test pulse type can be active at the same time.

If the test pulses shall be active during the integration of an image, the frequency should be 1 Hz or 10 Hz. With a frequency selection of 1 Hz also the switching rate should be changed to 10 seconds.

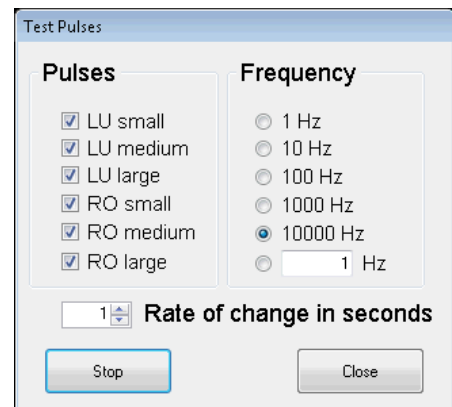


Fig. 3.7
Window “test pulses” of the program *HV-Control*.

3.6.1.3 Test pulse display

The window test pulse display shows averaged values for the X, Y and Z values from 1000 test pulses of the currently selected type. Also the standard deviation is calculated and multiplied by a factor 2.35 shown as DX, DY and DZ. This is a measure for the FWHM of the point spread function (see Eq. (2.4), p. 25). The X and Y values are given in pixel units, while the pulse height Z is converted to Volts (see oscillograph display).

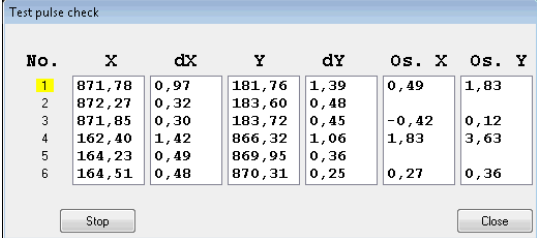


Fig. 3.8
Window “test pulse display” of the program *HV-Control*.

For this display it is important that the high voltage is switched off, as alone the MCP dark events would distort the evaluation of the test pulses.

3.6.1.4 Test pulse check

The test pulse check shows the same evaluation of the test pulses as the test pulse display, except that in this case all 6 test pulse types are switched on in sequence and the results are shown in a table. The number of the currently active test pulse is highlighted in yellow, so that it is easy to follow the current changes of the display.



No.	X	dX	Y	dY	Os. X	Os. Y
1	871,78	0,97	181,76	1,39	0,49	1,83
2	872,27	0,32	183,60	0,48		
3	871,85	0,30	183,72	0,45	-0,42	0,12
4	162,40	1,42	866,32	1,06	1,83	3,63
5	164,23	0,49	869,95	0,36		
6	164,51	0,48	870,31	0,25	0,27	0,36


Fig. 3.9
Window “test pulse check” of the program *HV-Control*.

Additionally the columns “Os. X” and “Os. Y” show the differences between successive X and Y values: $Os. X(1) = X(2) - X(1)$, $Os. X(3) = X(3) - X(2)$, accordingly for X(4) ... X(6) and for Y values. This highlights pulse height dependant variations which are caused usually by offset errors (see Chap. 2.5.4, p. 27).

As with the test pulse display it is important also in this case that the high voltage is switched off.

This display was also contained in the software of the ground station used during the 2nd *ORFEUS* flight. This helped in a fast functional verification of the whole detector electronics. In particular it could be verified, that the electronic resolution was the same as it was measured pre-flight.

3.6.1.5 Gain display



Gain [V]	Width [%]
2,97	101

Fig. 3.10
Window “gain display” of the program *HV-Control*.

The gain display shows the average of the Z coordinate of at least 1000 events (at rates above 1000 s^{-1} the measuring time is at least 1 second). The gain value is given in Volts (corresponding to the summed pulse signal shown on the oscillograph). The standard deviation is multiplied by a factor 2.35 and shown as a measure for the width of the distribution. It is given in percent of the gain value. Only in the case of a Gaussian distribution this value would correspond to the full width at half maximum (FWHM). In real pulse height distributions this value is only more or less a realistic FWHM.

This display is mainly used to adjust HV3 (see Fig. 3.6), which controls the MCP gain of the detector.

3.6.2 Data acquisition with program *Acquisition*

The program “*Acquisition*” is used for data acquisition and the integration of detector data. The main menu item “*Data*” (Fig. 3.11) contains several menu items to call different kinds of integration routines. The first four entries show the most important data acquisition functions. The numbers shown in parentheses correspond to the valid positions of the integration mode switch of the DPA (see Chap. 3.3, p. 35, and Fig. 3.3). If the integration mode switch is not in the correct position, the corresponding menu items are gray and not enabled.

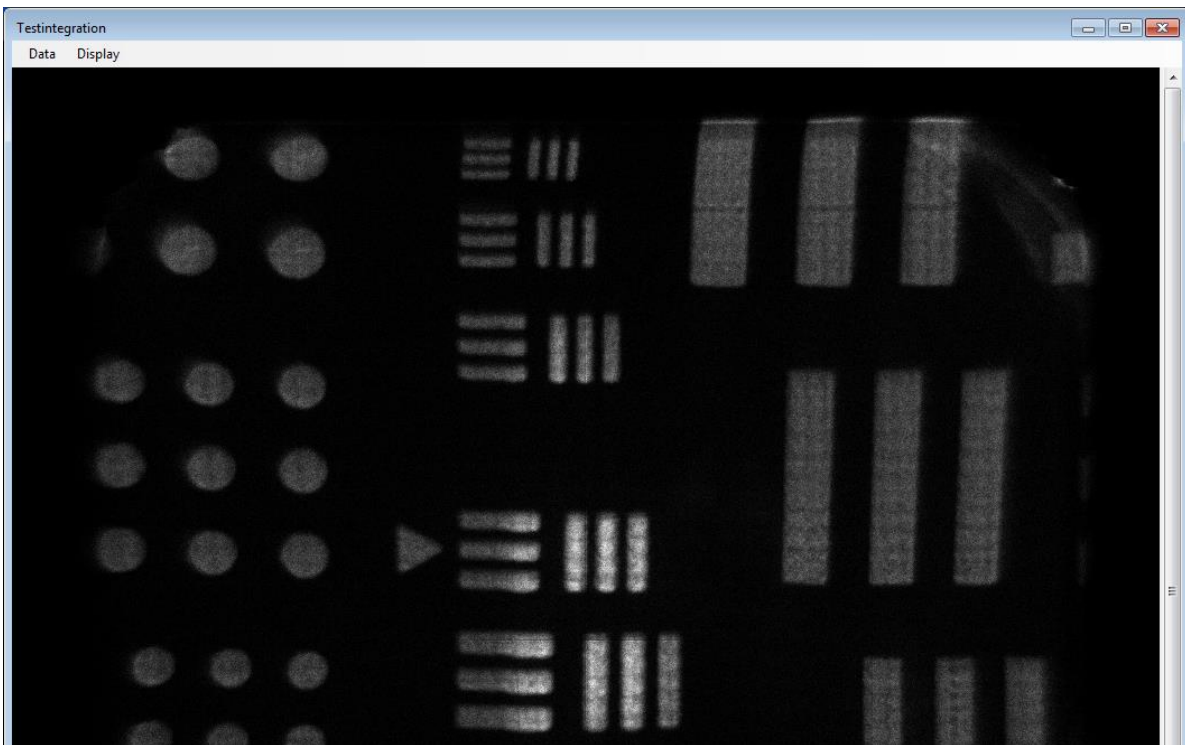


Fig. 3.12
Program *Data Acquisition* during the integration of an image.

3.6.2.1 Menu item *Image integration*

Menu item *Image integration* starts the integration of an image with a resolution of 1024 x 1024 pixels. The currently integrated image is updated every 10 seconds in the main window (Fig. 3.12). During integration the menu bar shows only the entries *Data* and *Display*. Some menu items allow for changing the image presentation on the screen (see Fig. 3.11). The integration is stopped with the button *Integration Stop* at the DPA (Fig. 3.3) or with the corresponding menu item in menu *Data*.

3.6.2.2 Menu item *Impulshöhe integrieren*

Menu item *Pulse height integration* starts the integration of a pulse height distribution. The currently integrated distribution is shown in a separate window (Fig. 3.13) which is updated every 10 seconds. The window may be drawn to an arbitrary size. A linear or a double logarithmic layout of the axes may be selected.

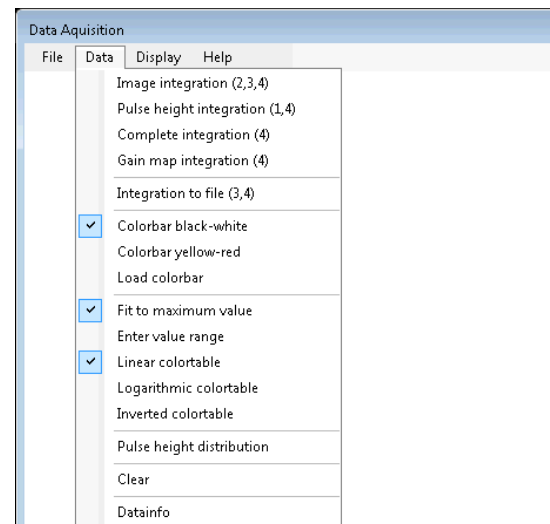


Fig. 3.11
Menu item *Data* of the program *Data Acquisition*.

3.6.2.3 Menu item *Complete integration*

Menu item *Complete integration* starts the integration of an image and a pulse height distribution at the same time.

3.6.2.4 Menu item *Gain map integration*

Menu item *Gain map integration* starts the integration of a gain map. The gain map shows for each pixel the averaged pulse height as intensity level. Internally the program makes use of 3 image memories: The first one integrates a normal photon image, in the second one the Z coordinates of each event are summed up and the third memory holds the ratio of pulse height sum to number of photons. Thus the averaged MCP gain over the detector area is imaged. The display may be toggled between gain map and photon image.

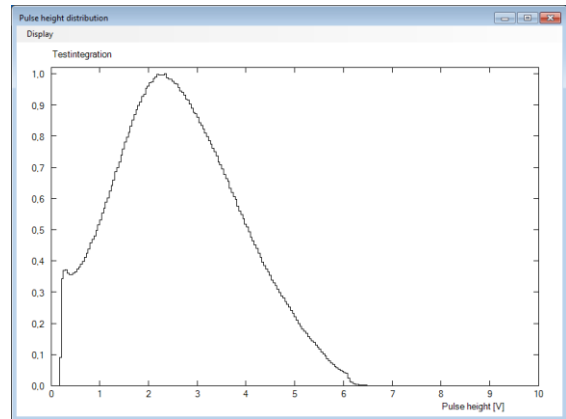


Fig. 3.13
Window of the pulse height distribution during the integration (linear layout of the axes).
X = pulse height in Volt
Y = relative occurrence

3.6.3 Program *Druck Center One*

The program *Druck Center One* records the pressure values of the pressure gauge *Center One* and of the sputter ion pump over a serial interface.

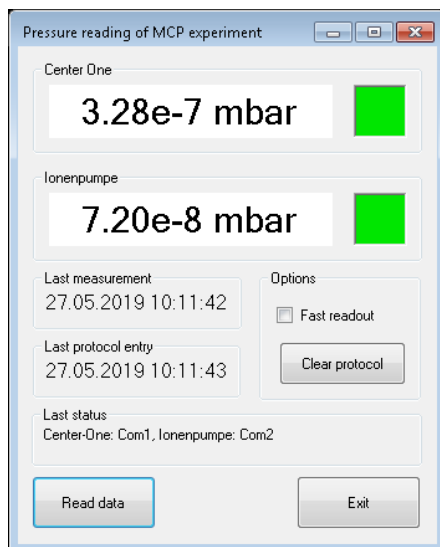


Fig. 3.14
Window of the program *Druck Center One*

Normally the program reads the values every minute. With the option *Fast readout* marked this happens every 5 seconds.

The button *Clear protocol* erases the current protocol file and creates a new one.

4 Experimentation

4.1 *Introductory notes*

During experimentation you should record your measurements in such a way, that you (and also the assistant) are able to understand the experiment from your records even much later. Therefore you should mark your notes with the corresponding chapter numbers of these experimental instructions and exercises. These notes have to be added to the final protocol. **Do read Chap. 4.13, S. 53, prior to carrying out the experimentation** and remember to note down all measured values with their corresponding units. **Please do not touch the lenses with your fingers!**

4.2 *Switch-on*

Carry out the following steps in the given order:

- If applicable switch on vacuum pump (it usually should run already), the vacuum should be better than 10^{-6} mbar. Check, that the detector valve is opened (screw should be unscrewed to the stop position, about 14 mm).
- If applicable switch on the Digital Position Analyzer
- If applicable switch on computer and log in
- Start programs *HV-Control* and *Druck Center One*
- Switch on power supply for the high voltage unit (switch at DPA, Fig. 3.3)
- Switch on oscillograph (device at the bottom of the rack)
- Switch on storage screen (device at the top of the rack, pull button at lower right, button *STORE* **not** pressed, if light point is visible: lower the beam intensity)
- In program *HV-Control*: Click to *Reset* in box *Over current*
- In program *HV-Control*: Call menu item *Delete protocol file ...*, to start with a new protocol file. Call menu item *Setup* and change in the box *Protocol settings* the update rate to 60 s.
- Program *Druck Center One*: click to *Clear protocol*
- Press button *Master Reset* at DPA
- Switch on the suction device for the UV lamp

4.3 *Test pulses*

We start with a checkout of the electronics. In program *HV-Control* call menu item *Test pulses* and start the test pulses. On the oscillograph screen you should see test pulses which change their height every second. On the storage screen the test pulse should change its position from one corner to the opposite one every 3 seconds. Measure the height of the test pulses (value of the maximum) by selecting only one test pulse in the window *Test pulses*. Note down the maximum voltage values for all 6 test pulse types.

Stop the test pulses and close the window *Test pulses*. Call the menu item *Testpulse display*. Note down the Z value (shown in V) for each test pulse type. Stop the test pulses and close the window *Testpulse display*.

Exercise 9:

Enter your measured values and the Z values for all test pulse types into a table. How good agree your measurements with the Z values? Calculate the differences between your measurements and the corresponding Z values and note these differences in percent.

Call the menu item *Testpulse check* and start the test pulses. After 2 (or more) runs do a snapshot of the window *Testpulse check*: Run program *PaintShop Pro*, click to the camera symbol, then use the right mouse button to click into the window *Testpulse check* (beforehand you should go to the menu item “Datei / Import / Schnappschuss / Setup...” and select the item “Fenster”).

Connect the detector housing to the vacuum pump with banana plug cables (normally the detector housing is isolated from the vacuum pump). Observe the values for the widths of the test pulses dX and dY. Make another snapshot and stop and close the test pulse check.

Exercise 10:

Print out the snapshots for your protocol. Describe the significant differences between the two measurements and mention the reason for these differences (if significant differences are visible).

Finally remove the banana plug cable connection again!

4.4 Switch-on of the high voltage

Remove all components except for lamp and condenser from the optical bench and position the condenser about 50 cm in front of the lamp. The double diffusor disc must be attached to the lamp. **Please do not touch the optical components with your fingers!**

Click to *HV unlock ...*, make sure, that the detector valve is opened, if so, select option *Vacuum valve is open!* and confirm by clicking *OK*. Now click **within 5 seconds** to the button *HV2 to HV4 on* (HV1 remains off). The high voltage is now switched on and the detector should produce pulses. Switch the count rate selection switch to position *Total Pulses*.

Switch on the lamp and press button *STORE* of the storage screen. It takes about one to two minutes until the lamp lights up in full intensity. During this time the count rate increases continuously. Adjust the count rate to a value of about $10,000 \text{ s}^{-1}$ by changing the condensers position. **The lamp may only be operated with suction (because of the ozone formation)!**

In program *HV-Control* open menu item *Gain display*. Also in program *HV-Control* click to button *Set ...* below **HV3** and change the high voltage value in steps of 10 V until a gain of 3.0 V is achieved. Note down the new high voltage value (also later every time you change this setting). Close the HV3 setup window and stop and close the gain display.

4.5 Dark current

Switch off the lamp and close the detector window by inserting the blind into the slot in front of the window. Switch the counting interval of the DPA counter to 10 s. Note down 10 counter values and calculate the average value. The counter display is valid when the green LED to the right of the counter display lights up; the value is displayed for 1 second.

4.6 What does solar blind mean?

Remove the blind in front of the detector window again. The detector is now exposed to ambient light and the count rate is higher than with absolute darkness. Note down 10 counter values (still at 10 s counting time). Again calculate the average value (in s^{-1}) and subtract the dark current value. Finally switch back the counting time to 1 s.

Use the lux meter to evaluate the illuminance at the detector surface. Hold the measuring cell directly in front of the detector and measure the illuminance in lux.

The illuminance in lux (= lumen/m²) is a photometric quantity which takes into account the spectral sensitivity of the eye (luminosity function, Fig. 4.1). The illuminance has to be converted approximately into a physical quantity (irradiance in Watt/m²). The conversion factor (in lumen/Watt) is called luminous efficacy and is wavelength dependant (Fig. 4.1).

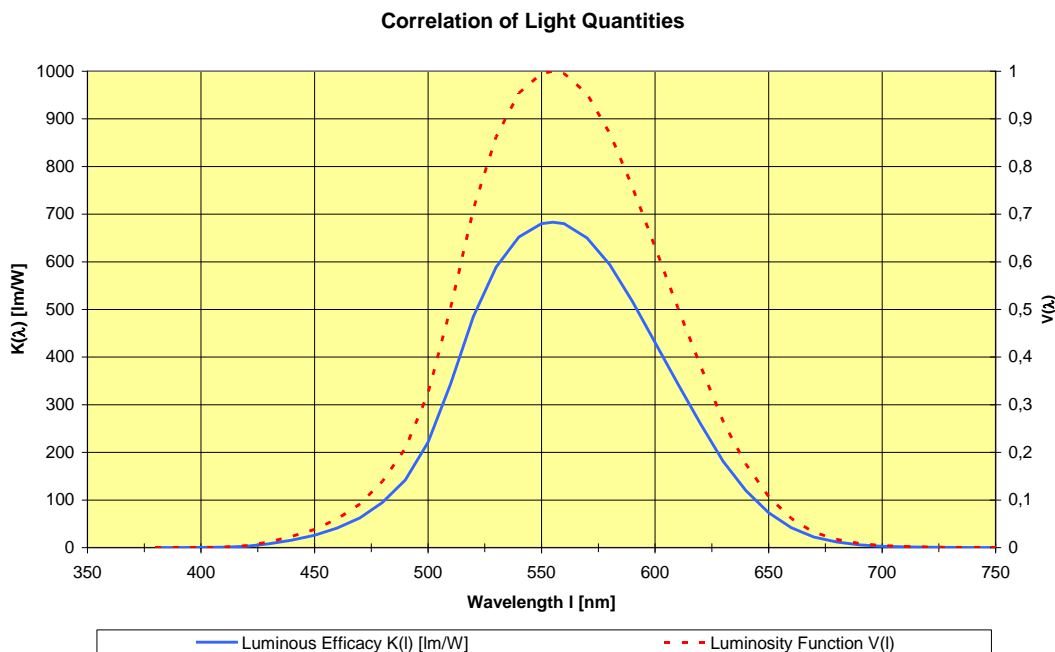


Fig. 4.1

Correlation between photometric and physical light quantities

(source: <http://www.reitmayer.de/phligroe.html> (outdated), see also: Heinrich Reitmayer, Dissertation, TU München, 2000).

Exercise 11:

Indicate the count rate produced by the ambient light in counts/s.

Estimate from Fig. 4.1 a reasonably averaged value for the luminous efficacy under the given light conditions.

Also give a reasonable average wavelength for the ambient light. Evaluate from these values the number of photons hitting the detector. Calculate from this the averaged sensitivity (quantum efficiency) of the detector for visible light.

How many pulses would a 1 mW He-Ne laser thus approximately produce on a detector with this sensitivity (if the sensitivity were not wavelength dependant)?

4.7 Pulse height distribution

4.7.1 Full image

Switch on the lamp again and open the window *Gain display*. Adjust HV3 such that the gain is at 3.0 V again. Note down the values for gain and width **before and after** the following pulse height integrations. Switch off the gain display during the pulse height integration.

Switch the integration mode switch at DPA to position 4 (x, y, t, z). **Remember to reset the DPA time counter prior to each integration.** Call program *Data acquisition* and start a pulse height integration (see Chap. 3.6.2.2, p. 40). Stop the integration, when the curve is sufficiently smooth (about 200 s). Save the graph of the pulse height distribution with the menu item *Display / Save bitmap*. Don't forget the second measurement of the gain display!

4.7.2 Partial image

Select a partial image at the DPA (Image Window: X=2, Y=0) and do the pulse height integration again. Don't forget to note down gain and width **before and after** pulse height integration and save the graphics. **Finally select image window again as X=9, Y=9 (full image).**

Exercise 12:

Use the plots of the pulse height distributions to estimate the position of the maximum and the geometric FWHM. You should draw these quantities in the plots, measure the values in cm and give a conversion factor in V/cm to calculate the values in V. Give the FWHM in percent of the maximum position.

What is the reason for differences (maximum and FWHM) between full image and partial image measurements? Compare the graphically estimated values for gain and width with those noted from the gain display. Why differ the computer values (use averages of the measurements before and after integration) for gain and width from the graphically estimated values? How calculates the computer the values for gain and width?

4.8 Outgassing

In program *HV-Control* select menu item *Setup* and change the update rate for the protocol file to 5 s and activate option *Fast readout* in program *Druck Center One*. Start the *Gain display* and adjust HV3 until a gain of 3 V is achieved. **Leave the gain display active during this measurement**, so that the gain values are automatically written into the protocol file.

Move the condenser slowly towards the lamp until a count rate (Total Pulses) of $50,000 \text{ s}^{-1}$ is achieved. After 5 minutes regulate the count rate back to $10,000 \text{ s}^{-1}$ and wait again 5 minutes (in the meantime you

might deal already with Exercise 14). **Finally set the update rate back to 60 s** (*HV-Control* and *Druck Center One*) and stop and close the gain display.

Open Excel file *Protokoll_eng.xls* and run macro “*ProtokollImport*”. This imports the current protocol file of the program *HV-Control*. The already prepared diagrams are automatically updated.

Exercise 13:

Show the chronological course of the gain and the pressure in a diagram and print it. Comment on the result: Why increases the pressure? Why decreases the gain? What happens when the count rate is reduced again to $10,000\text{ s}^{-1}$?

4.9 Flat field and gain map

Remove the large diffuser from the protective housing and mount it in front of the detector window. Regulate the count rate to a value of about $20,000\text{ s}^{-1}$. Adjust the gain to about 3 V.

Start a *Gain map integration* (see Chap. 3.6.2.4, p. 41). Fill in the integration parameters in the start window and enter a unique filename.

The integration should last at least as long as it takes to achieve a signal to noise ratio of 10 for the exposed parts of the image. It is advisable to run this integration during lunch time.

Exercise 14:

Which value per pixel do you need for a signal to noise ratio of 10? Calculate the necessary integration time from the rate of the **Active Pulses** (about 900×900 exposed pixels). Use IDL and the program “*auswertung*” to produce printouts of the images. (Set screen properties to 256 colours!)

4.9.1 Homogeneity

This data analysis may be skipped initially and carried out after finishing all measurements.

Evaluate the small scale homogeneity of the flatfield image. For that purpose produce a histogram of an image section which seems to be rather homogeneous in its intensity distribution (IDL program “*auswertung*”, menu item “*Auswertung/ Statistik fuer Bildausschnitt*”) and make a printout of this histogram (menu item “*Export/Plot-Hardcopy*”).

If the intensity variations from pixel to pixel were solely due to statistical variations, the histogram should coincide with a Poisson distribution. As the mean value is rather large (~ 100) and also the

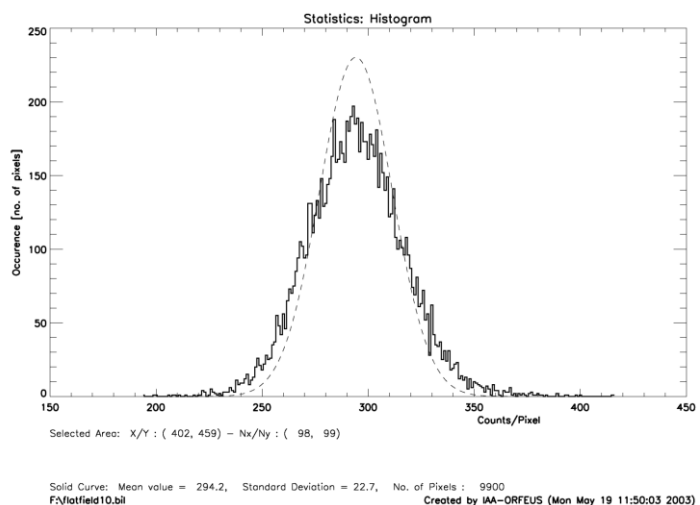


Fig. 4.2
Histogram of the intensity distribution of an image section.
The dashed curve represents a Poisson distribution with the same mean value.
The values printed in the plot refer to the measured values, not to the theoretical curve!

number of measured values is large (= number of pixels), the Poisson distribution may be approximated very well by a Gaussian distribution (with $\sigma = \sqrt{\text{mean value}}$).

Fig. 4.2 shows such a histogram. The dashed curve shows a Gaussian distribution with the same mean value. One can see that the theoretical curve does not exactly coincide with the measured histogram. Thus the intensity variations from pixel to pixel are not solely due to statistical variations. There are also systematic errors; therefore the homogeneity is not optimal.

Exercise 15:

Evaluate the homogeneity within the selected image section by comparing the measured histogram with the theoretical Gaussian distribution drawn in the plot. Give the exact complete formula for this dashed Gaussian curve plotted on your printout (3 parameters, which can be estimated from the numbers printed on your plot!) and check your formula by calculation of 2 numbers (one in the slope of the curve and the other near the maximum – draw the values in your printout). Justify the numbers used for the 3 parameters of your formula.

4.10 Determination of the focal length by the Bessel method

Position the condenser about 50 cm in front of the lamp, remove afterwards the diffusion disc in front of the detector and position the optical components on the optical bench as follows:

- lamp with double diffusion disc, small iris diaphragm in front of lamp
- test mask, about 90 cm away from the front of the detector housing
- condenser in 25 cm distance to lamp
- quartz lens between detector and test mask, iris diameter 35 mm, closer to the test mask than to the detector

The determination of the focal length by the Bessel method is based on the fact, that for a given distance e between object and image plane, which is larger than the fourfold focal length, there exist two lens positions at which the object is sharply imaged in the image plane. If the distance between these two lens positions is determined as d , the focal length f of a thin lens can be estimated from the following formula (Bergmann / Schäfer, 1962):

$$f = \frac{e^2 - d^2}{4e} \quad (4.1)$$

First of all determine the distance e between test mask and MCP surface. For this purpose you measure the distance between test mask and front side of the (gold-coloured) detector housing (all distances measured to an accuracy of 1 mm). Now add the distance from the detector housing to the MCP surface; its optical length of 25 mm is calculated as follows: The mechanical distance equals 26.7 mm. The quartz window has a thickness of 5 mm; the index of refraction for quartz is $n = 1.5$ at a wavelength of 254 nm. Thus the optical path length is only $5 \text{ mm} / 1.5 = 3.3 \text{ mm}$, which is a shortening by 1.7 mm. Therefore you get the value e by **adding to the distance test mask – front side a length of 25 mm**.

Next you have to determine the two lens positions at which a sharp imaging is achieved. Start with the position near the test mask. Firstly focus the image by observing the real time image on the storage

screen. Adjust the count rate to about $10,000 \text{ s}^{-1}$ by changing the small iris diaphragm. Afterwards you start an image integration for a certain time (e.g. 100 s). Stop the integration after that time and make a screen shot with PaintShop Pro from a relevant image section (beforehand you should call once the menu item “Datei / Import / Schnappschuss / Setup...” and select the option “Fensterinhalt”) – crop the imported image to a meaningful area. Subsequently move the lens by 2 mm and note down the corresponding lens position on the scale of the optical bench (you best use the edge of the slider facing towards the lamp). Integrate for the same time as before and again make a snapshot of the same image section. Compare these sections and decide from this into which direction you have to move the lens next. Repeat these steps until you have found the optimal lens position.

Determine the rough lens position located near the detector. Then set the count rate to 3000 s^{-1} . Determine the correct lens position as described above. Calculate the distance between the two optimal slider positions on the optical bench: This is your value d .

In addition to this determine the focal length also for visible light by displaying a very far object on a screen.

Exercise 16:

Calculate the focal length of the lens for a wavelength of 254 nm according to Eq. (4.1). Compare this value to the focal length measured with visible light. What is the reason for the difference?

4.11 Dead time and efficiency

Move the condenser towards the lamp until a count rate (Total Pulses) of about $100,000 \text{ s}^{-1}$ is achieved. The vacuum pressure should not exceed $1-2 \cdot 10^{-6} \text{ mbar}$, otherwise the automatic pressure monitoring would switch off the high voltage!

Note down the counter values for total pulses, active pulses and both discriminator thresholds. Reduce the count rate (Total Pulses) in steps of $10,000 \text{ s}^{-1}$ by moving the condenser and note down each time all four counter values (additionally measure also at $75,000 \text{ s}^{-1}$).

Important:

During read-out of the counter values for the active pulses the gain display must not be active!

Exercise 17:

Create an Excel table from the measured values. Calculate for “Total Pulses” and “Lower Threshold” a dead time correction according to Eq. (2.24), p. 32, with a counter dead time of $2 \mu\text{s}$. Calculate the efficiency = (active pulses) / (lower threshold – upper threshold).

Calculate theoretical values for the efficiency according to Eq. (2.22), p. 31 (see Fig. 2.29). Present the values in a diagram. Use the (detector) dead time as parameter, which is stored in a separate table cell. Change this value until the theoretical curve fits the measured curve well.

Determine n_{max} for this dead time with Eq. (2.23), p. 31. Compare n_{max} with your maximum value for active pulses.

4.12 Linearity calibration

4.12.1 Setup

Alter the setup of the optical bench as follows:

- Replace the diffusion disc in front of the lamp by a pinhole aperture plate. For this purpose switch off the lamp!
- Remove the condenser and position the lens 17.5 cm in front of the lamp (iris diaphragm open!).
- Insert the test mask consisting of three vertical and horizontal pinhole lines into the slot in front of the detector window. The line pattern of this test mask is composed from pinholes, which have a diameter of 0.2 mm and a distance of 0.5 mm. In order to be able to identify the orientation of the mask, the lettering **AIT** is added in the lower right quarter, also made from pinhole lines.

Switch on the lamp. A count rate of more than 300 s^{-1} should be achieved. The intensity should be preferably equally distributed over all lines (check on the storage screen).

4.12.2 Measurement

If necessary set MCP gain to 3 V again. Integrate an image for 15 minutes. Save the image in your group directory.

Hint:

As your measurements are finished with it, you should switch off the high voltage in program “*HV-Control*” after completion of the integration. Afterwards switch off the oscillograph, the lamp and the HV power supply at the DPA. Set the update rate of the protocol file back to 3600 s.

For data analysis with the IDL program “*auswertung*” first set the screen setup to a colour depth of 256 colours, otherwise the colour display in IDL would not work correctly.

Start IDL and call the program “*auswertung*”. This program was originally used for the data analysis of the *ORFEUS* measurements. Load the just integrated image.

You should now determine the X positions of the pinholes of the middle horizontal line and estimate from these the (non-)linearity of the detector. For this purpose you have to extract intensity profiles piece by piece along this line. Afterwards you fit a series of Gaussian curves to each of the plotted intensity profiles. The centres of the

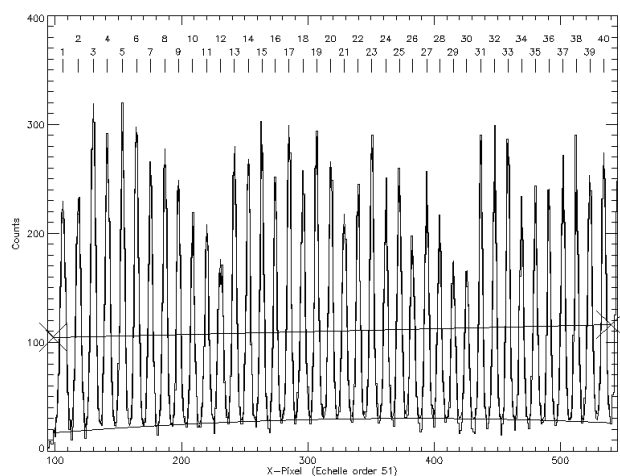


Fig. 4.3
Intensity profile along a pinhole line. 40 Gaussian curves were fitted to this profile. The background was fitted as parabola.

Gaussian curves are the measured positions of the pinholes.

The program “*auswertung*” can plot an intensity profile (“*Schnitt*”) for a given start and stop point. At arbitrary points several Gaussian curves may be fitted to this plot. The data of the Gaussian curves are automatically written to a protocol file (you must not close the program and start it again, as this would create a new protocol file).

Plot intensity profiles which contain 40 points of the line. For each of these profiles you have to execute a automatic Gaussian fit. Thus you can estimate the centres of all about 80 points along the middle horizontal line. Proceed as follows:

- Check under menu item “*Einstellungen/Plot-Eichung*” that the option “*X=Pixel, Y=Counts*” is selected.
- Call the menu item “*Auswertung/Schnitt*”.
- In the image first click to the (left) start point and afterwards to the (right) end point of the intensity profile to be plotted. This extracts an intensity profile from the image, which covers a pre-set width (to be selected with menu item “*Einstellungen/ Schnittbreite*”). An odd width from 11 to 21 pixels is reasonable. This assures that the pinhole images are captured in full width.
- Afterwards call menu item “*Auswertung/Auto-Gaussfit ueber Schnitt*”.
- In the plot window you first have to mark (using the left mouse button) the left position: The x-position should mark the first (left) minimum and the x-position should be at about half the height between minimum and maximum. Then mark to the last (right) position. The points you have clicked are marked with tilted crosses (see Fig. 4.3). Make sure that the line connecting the two marks crosses all peaks once. To end the definition of the Gaussian fit use the **right** mouse button to click into the plot window. The fitted curve will be drawn into the plot window (Fig. 4.3). Check that all maxima are fitted correctly. Erroneous fits may be just repeated again. Therefore use menu item “*Auswertung/letzten Schnitt wiederholen*” to update the plot window and afterwards repeat the automatic Gaussian fitting.

After all pinhole positions are estimated stop the program and IDL and copy the file *logfile.txt* from the directory *C:\Benutzer\prakt* into your group directory.

4.12.3 Analysis

For each Gaussian fit carried out the following entries are contained in file *logfile.txt*:

```
Kurve Nr. 1:
Schwerpunkt   :          97.196253   =   1107.9357 A
Amplitude     :          58.749829
Breite (FWHM):          5.2349586   =   0.15797641 A
Wl / d Wl     :          7013.2984
```

Important for your analysis is only the entry marked “*Schwerpunkt*”, this denotes the centre of the Gaussian curve in pixels (and also converted to a wavelength in Å). These pixel positions are your measured values. The corresponding true positions are the centres of the pinholes in the mask, which have a distance of 0.5 mm from each other. **If you had repeated a certain fit, you have to remove the invalid entries with a text editor.** Check that all entries are available (all points should have nearly the same distance; all points should be sorted in ascending order).

For analysis open the Excel file *Auswertung_Linearitaet_eng.xls* which should be already in your group directory. Use the macro “*Linearitaetsmessung_importieren*” to import the file *logfile.txt*. In column “*Pixel-Position*” all measured Gaussian centres are entered in ascending order. Column “*True position [mm]*” is filled with values increasing by 0.5 mm, starting at 0 mm. The other columns are filled with formulae in the first row. These formulae are copied to the other rows for as many of rows as measured values are available. This applies to the following columns:

- “*Straight line [Pixel]*”: This column shows values for a straight line used as reference for the measured values. By calculating the difference the deviation of the measured values from a straight line can be more easily seen. The two line parameters *slope* and *border value* are automatically determined and filled into cells B2 and B3. You also may change these values and may later use the button “*estimate straight line*” to estimate the values again. Also have a look to the sheet **Diagramm 2**.
- “*Difference (Measurement – straight line)*”: Here the differences between measured values and calculated straight line are entered. This column is shown in the diagram as “*Measurement*”. If you change the line parameters, you should select them such that the measured values show a symmetrical curve in the diagram (see Fig. 4.4). This curve is shown in the sheet **Diagramm 1**.

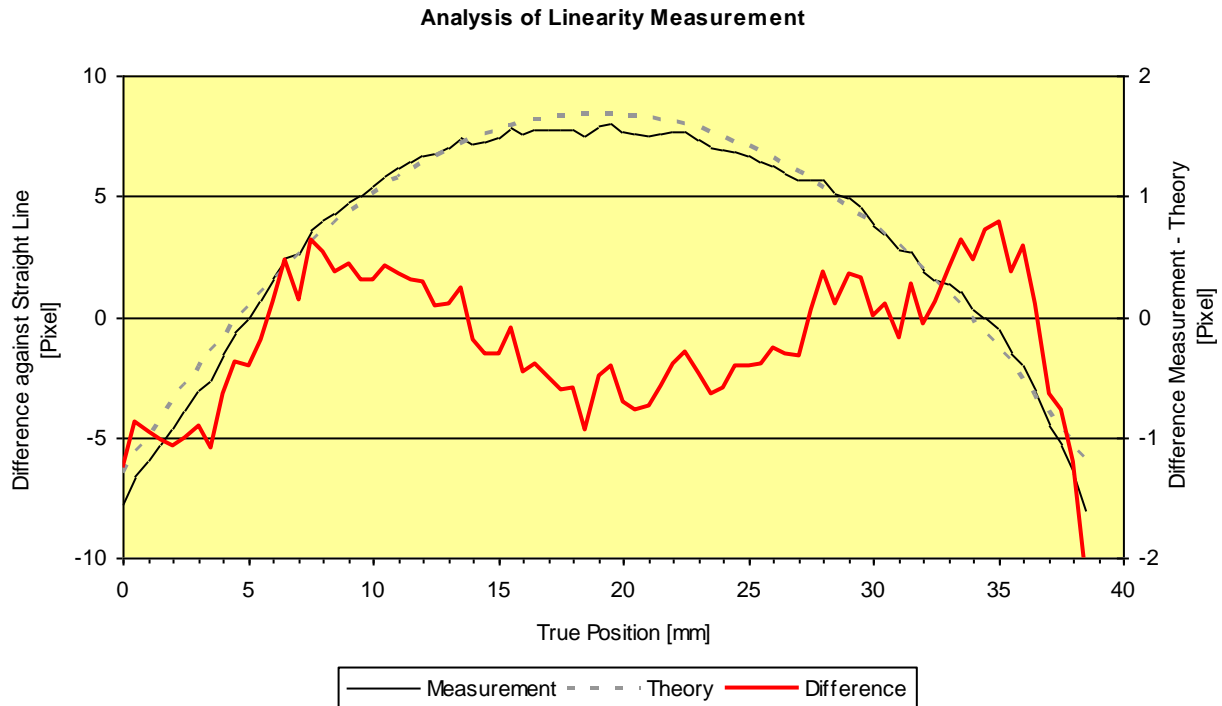
Now you should produce a theoretical calibration curve by selecting the two parameters cross talk (b , see Chap. 2.5.3, p. 26) and gain difference (a , see Chap. 2.5.3, p. 26). Vary the parameters such that the theoretical curve fits the measured curve as good as possible. Note that parameter b (“*Cross talk*”) changes the slope of the theoretical curve, while parameter a (“*Gain difference*”) determines its curvature. As the zero point of the true position is selected arbitrarily, a further parameter has to be envisaged: a zero point shift. The following columns calculate the theoretical values (comprehend the Excel formulae at the screen):

- “*Theory (Cross talk)*”: This column contains the formula from equation (2.10). As x is in this formula a normalised value between 0 and 1, we have to relate the true position to the active anode width of 44 mm. Thus the true position is corrected by the zero position shift and then divided by 44. To keep the formula more clearly the expressions $1-b$ and $1+b$ were put in cells D5 and F5.
- “*Theory (Gain difference)*”: This column contains the formula from equation (2.12). As input value x the result from the previous calculation in column F is taken, which is already normalised. To make the final result comparable to the measured pixel values, we have to multiply the normalised result x' with the maximum pixel value of 1023.
- “*Theory – Straight line*”: This column corresponds to the values (measurement - straight line) and is shown also in the diagram. The parameters for gain difference, cross talk and zero point shift are to be chosen such that both curves fit as good as possible. To be able to judge the quality of the fit, the next column shows the difference to the measured values.
- “*Measurement - Theory*”: This column is also shown in the diagram, but with its own Y-axis. Thus differences between the two curves can be seen more clearly (see Fig. 4.4). The three parameters should be chosen such that this curve is as closely to zero as possible.

As for each change of the parameters a and b also the value for the zero point shift changes, this value has

Exercise 18:

Create the Excel file as described and select the optimal fit parameters (your diagram should look similar to Fig. 4.4). Print out your diagram and note down all parameters.

**Fig. 4.4**

Excel diagram of the analysis of the linearity measurement. Your diagram should look similar to this one, if you have chosen the parameters correctly. Left axis: gray curves, right axis: red curve.

to be adjusted regularly. For this purpose there is the button “*calculate zero point*”. A click to this button shifts the red difference curve back to the centre of the diagram.

4.12.4 Carrying out the correction

For analysis of the *ORFEUS II* data not only the linearity calibration had to be carried out, but also a wavelength calibration, as the X axis of the detector image was the dispersion direction of the Echelle spectra. Therefore also a theoretical formula exists, the parameters of which had to be fitted as well. This fit was not done manually, but by a computer program. For this purpose 814 narrow interstellar absorption lines were identified in the *ORFEUS II* Echelle spectra and finally 7 calibration parameters for the wavelength calibration were determined by fitting (Barnstedt et al. 1999).

For the *ORFEUS* spectra each X pixel value was assigned to a corresponding wavelength value; redistribution to new “spectral pixels” was not necessary. However, if the detector were used mainly to record images, it might be necessary to straighten the images, i.e. to calculate a corrected image. Therefore you have to know the inverse function of the above mentioned calibration. Thus you have to assign each pixel in the **measured** image to the **original** position in pixel units.

Actually it is not sufficient, to assign a new position to each pixel. Instead, the original positions have to be calculated for each of the four corners of a pixel and then the measured pixel has to be projected onto the new pixel raster. The intensity of the measured pixel has to be distributed pro-rata over all affected new pixels. Thus intensity variations caused by local image distortions are also removed.

Exercise 19:

Determine the formula for calculating a corrected image. Starting with an x -value (pixel number) of the measured image the formula shall give the resulting x -value in pixel units for the corrected image. The formula sought-after is the inverse function of the formulae given in the Excel columns “Gain difference” and “Cross talk” according to equations (2.10) and (2.12).

4.13 Hints for writing a protocol

The following information should be given at the beginning of the protocol:

- Date of the experiment
- Name of the experiment
- Number of your group
- Names (author of the protocol underlined)

The protocol should be written in such a way that an outsider can use the protocol to understand what has been done in each part of the experiment. In addition to a brief description of the most important basics, a brief description of the setup and the execution of each part of the experiment should be given. The measured values obtained are to be listed, as well as the calculations necessary for the analysis with all numerical values used and their units.

The individual sections of the protocol should be numbered according to the chapter numbers of this manual and the numbers of the exercises, respectively.

The following points have to be considered when noting down the measurements and carrying out the calculations:

1. As a basic principle measured values have given as their original reading (i.e. for oscillographs the reading in scale units [DIV]), if applicable together with the corresponding calibration of the instrument (i.e. sensitivity of the oscillograph in [V/DIV]). In a second column the estimated values with their corresponding units have to be given (values in V in the above mentioned example).
2. All measured values as well as all calculated values have to be given with their corresponding units (in the case of tables the units shall be given in the header row).
3. For all calculated values the corresponding formula and all used values and constants (including units) shall be given. The ansatz or method of calculation should be described shortly in words (unless obvious).
4. For calculated values only those decimals shall be given, which correspond to the accuracy of the measurement. (At 1% measuring accuracy a calculated value shall not be given as 12.34567 but as 12.3, and correspondingly a value of e.g. 23 as 23.0).
5. For the evaluation of diagrams all reference lines have to be drawn into the diagram. The reading values (usually in centimetres) shall be given, together with a calibration factor, which has to be estimated from the diagram.
6. The parameters estimated in Excel sheets have to be noted explicitly in the protocol.
7. The diagrams printed out during the experiment shall be labelled and shall be attached to the protocol. Also the original notes written during the experiment shall be attached to the protocol.
8. The results shall be presented in written text (whole sentences!).
9. The text should refer to tables and diagrams. Tables have headlines, diagrams have captions.
10. Before the protocol is handed over it should be read and corrected, if necessary, by the other group members. Make use of a spell checker.

11. It is very helpful, if the protocol is written promptly after the experiment was carried out.
12. The original notes are part of the protocol – please add these original sheets to the protocol (at electronic submission of the protocol please add scans of the original sheets).

5 Literature and sources

Books which are important for the preparation are marked in bold face.

- Appenzeller, I., Krautter, J., Mandel, H., Östreicher, R.: *ORFEUS focal plane instrumentation - Echelle-spectrograph*. ESA SP-281, Vol. 2, 1988, 337-339
- Barnstedt, J.: *Entwicklung eines photonenzählenden transportablen Kamerasystems für astronomische Anwendungen im sichtbaren Spektralbereich*. Dissertation Tübingen 1985
- Barnstedt, J., Kappelmann, N., Appenzeller, I., Fromm, A., Gölz, M., Grewing, M., Gringel, W., Haas, C., Hopfensitz, W., Krämer, G., Krautter, J., Lindenberger, A., Mandel, H., Widmann, H.: *The ORFEUS II Echelle Spectrometer: Instrument Description, Performance and Data Reduction*. Astronomy & Astrophysics Suppl. Ser. **134**, 1999, 561-568
- Barnstedt, J., Gringel, W., Kappelmann, N., Grewing, M.: *The ORFEUS II Echelle Spectrum of HD 93521: A reference for interstellar molecular hydrogen*. Astronomy & Astrophysics Suppl. Ser. **143**, 2000, 193-210
- Bergmann, L., Schaefer, C.: *Lehrbuch der Experimentalphysik, III. Band, I. Teil (Wellenoptik)*, 3. Auflage, Walter de Gruyter & Co., 1962**
- Brandt, S.: *Datenanalyse*, 3. Auflage, BI-Wissenschaftsverlag, 1992
- Danks, A.C., Joseph, C., Bybee, R., Argebright, V., Abraham, J., Kimble, R., and Woodgate, B.: *The STIS MAMA Status: Current Detector Performance*. ESA SP-356, 1992, 269-274
- Fraser, G.W.: *X-Ray Detectors in Astronomy*. Cambridge University Press 1989 (Kapitel 3: Microchannel Plates, S. 116)
- Grewing, M., Appenzeller, I., Barnstedt, J., Bowyer, S., Hurwitz, M., Krämer, G., Kappelmann, N., Krautter, J., Mandel, H.: *ORFEUS*. ESA SP-413, 1998, 757-762
- Hamamatsu Photonics K.K.: *Characteristics and Applications of Microchannel Plates*. Technical Manual RES-0795
- Hurwitz, M., Bowyer, S.: *ORFEUS focal plane instrumentation: The Berkeley spectrometer*. ESA SP-281, Vol. 2, 1988, 329-331
- Knapp, G.: *Crossed grid anode and its image partitioning*. Rev. Sci. Instrum. **49**, 1978, 982-987
- Krämer, G., Eberhard, N., Grewing, M., Gringel, W., Haas, C., Kaelble, A., Kappelmann, N., Petrik, J., Riegger, J.: *ORFEUS: A 1m-EUV/FUV telescope on the space platform ASTROSPAS*. ESA SP-281, Vol. 2, 1988, 333-336

- Lampton, M., and Carlson, C.W.: *Low-distortion resistive anodes for two-dimensional position-sensitive MCP systems*. Rev. Sci. Instrum. **50**, 1979, 1093-1097
- Lampton, M., Siegmund, O., and Raffanti, R.: *Delay line anodes for microchannel-plate spectrometers*. Rev. Sci. Instrum. **58**, 1987, 2298-2305
- Martin, C., Jelinsky, P., Lampton, M., Malina, R.F., Anger, H.O.: *Wedge-and-strip anodes for centroid-finding position-sensitive photon and particle detectors*. Rev. Sci. Instrum. **52**, 1981, 1067-1074
- Siegmund, O.H.W., Gummin, M.A., Stock, J., and Marsh, D.: *Microchannel plate imaging detectors for the ultraviolet*. ESA SP-356, 1992, 89-96
- Tietze, U., Schenk, Ch.:** *Halbleiter-Schaltungstechnik*. 10. Auflage, Springer Verlag, 1993
- Vallerga, J.V., Gibson, J.L., Siegmund, O.H.W., Vedder, P.W.: *Flat field response of the microchannel plate detectors used on the Extreme Ultraviolet Explorer*. In: EUV, X-ray, and gamma-ray instrumentation for astronomy and atomic physics, Proc. SPIE **1159**, 1989, 382-391
- VALVO: *Technische Informationen für die Industrie, Microchannel plates*. 1976
- Weinzierl, P., Drosch, M.: *Lehrbuch der Nuklearelektronik*. Springer-Verlag 1970
- Wiza, J. L.: *Microchannel Plate Detectors*. Nucl. Instr. Meth. **162**, 1979, 587-601

List of *ORFEUS* publications:

<http://www.uni-tuebingen.de/de/4530>

6 Appendix: Natural constants

Quantity	Symbol	Value
Vacuum velocity of light	c	$2,99792458 \cdot 10^8 \frac{m}{s}$
Elementary charge	e	$1,60217733 \cdot 10^{-19} C$
Planck's constant	h	$6,6260755 \cdot 10^{-34} J \cdot s$ $4,1356693 \cdot 10^{-15} eV \cdot s$
Electrical field constant (Permittivity of the vacuum)	ϵ_0	$8,854187871 \cdot 10^{-12} \frac{A \cdot s}{V \cdot m}$